

FINAL REPORT ~ FHWA-OK-14-13

# DEVELOPMENT AND IMPLEMENTATION OF A MECHANISTIC AND EMPIRICAL DESIGN GUIDE (MEPDG) FOR RIGID PAVEMENTS — PHASE 2

M. Tyler Ley, Ph.D., P.E.  
Amir Hajibabaei  
Morteza Khatibmasjedi  
School of Civil and Environmental Engineering  
College of Engineering, Architecture and  
Technology  
Oklahoma State University

October 2014



The contents of this report reflect the views of the author(s) who is responsible for the facts and the accuracy of the data presented herein. The contents do not necessarily reflect the views of the Oklahoma Department of Transportation or the Federal Highway Administration. This report does not constitute a standard, specification, or regulation. While trade names may be used in this report, it is not intended as an endorsement of any machine, contractor, process, or product.

**DEVELOPMENT AND IMPLEMENTATION OF A MECHANISTIC  
AND EMPIRICAL PAVEMENT DESIGN GUIDE (MEPDG) FOR  
RIGID PAVEMENTS – PHASE 2**

**FINAL REPORT ~ FHWA-OK-14-13**  
ODOT SP&R ITEM NUMBER 2208

**Submitted to:**

John R. Bowman, P.E.  
Director of Capital Programs  
Oklahoma Department of Transportation

**Submitted by:**

M. Tyler Ley, Ph.D., P.E.  
Amir Hajibabaei, Graduate student  
Morteza Khatibmasjedi, Graduate student  
School of Civil and Environmental Engineering  
Oklahoma State University



October 2014

# TECHNICAL REPORT DOCUMENTATION PAGE

<b>1. Report No.</b> FHWA-OK-14-13	<b>2. Government Accession No.</b>	<b>3. Recipient's Catalog No.</b>	
<b>4. Title and Subtitle</b> Development and Implementation of a Mechanistic and Empirical Pavement Design Guide (MEPDG) For Rigid Pavements – Phase 2		<b>5. Report Date</b> October 2014	
		<b>6. Performing Organization Code</b>	
<b>7. Author(s)</b> Tyler Ley, Amir Hajibabae, Morteza Khatibmasjedi		<b>8. Performing Organization Report No.</b>	
<b>9. Performing Organization Name and Address</b> Oklahoma State University School of Civil and Environmental Engineering 207 Engineering South Stillwater, OK 74078		<b>10. Work Unit No. (TR AIS)</b>	
		<b>11. Contract or Grant No.</b> ODOT SP&R item Number 2208	
<b>12. Sponsoring Organization Name and Address</b> Oklahoma Department of Transportation Materials and Research Division 200 N.E. 21 <sup>st</sup> Street, Room 3A7 Oklahoma City, OK 73104		<b>13. Type of Report and Period Covered</b> Final Report October 2012 – October 2014	
		<b>14. Sponsoring Agency Code</b>	
<b>15. Supplementary Notes</b>			
<b>16. Abstract</b>  The work investigates the impact of curing methods and their impact on subsequent curling in both the laboratory and the field in different drying environments. Results are also presented for a field instrumentation of a CRCP pavement in Tulsa, Oklahoma that uses a number of different curing methods. Next, a sensitivity analysis is completed for typical Oklahoma jointed and continuously reinforced pavements with different base friction parameters. Then the results from Darwin-ME are compared with field performance of CRCP and JPC pavements in Oklahoma. Finally, the shrinkage and coefficient of thermal expansion of concrete pavement mixtures are investigated with different past contents.			
<b>17. KEY WORDS</b> Concrete, Pavement, Darwin-ME, MEPDG		<b>18. Distribution Statement</b> No restrictions. This publication is available from the Materials & Research Division, Oklahoma DOT.	
<b>19. Security Classification (of this report)</b> Unclassified.	<b>20. Security Classification (of this page)</b> Unclassified.	<b>21. No. of Pages</b> 87	<b>22. Price</b> N/A

## SI\* (MODERN METRIC) CONVERSION FACTORS

APPROXIMATE CONVERSIONS TO SI UNITS				
SYMBOL	WHEN YOU KNOW	MULTIPLY BY	TO FIND	SYMBOL
LENGTH				
in	inches	25.4	millimeters	mm
ft	feet	0.305	meters	m
yd	yards	0.914	meters	m
mi	miles	1.61	kilometers	km
AREA				
in <sup>2</sup>	square inches	645.2	square millimeters	mm <sup>2</sup>
ft <sup>2</sup>	square feet	0.093	square meters	m <sup>2</sup>
yd <sup>2</sup>	square yard	0.836	square meters	m <sup>2</sup>
ac	acres	0.405	hectares	ha
mi <sup>2</sup>	square miles	2.59	square kilometers	km <sup>2</sup>
VOLUME				
fl oz	fluid ounces	29.57	milliliters	mL
gal	gallons	3.785	liters	L
ft <sup>3</sup>	cubic feet	0.028	cubic meters	m <sup>3</sup>
yd <sup>3</sup>	cubic yards	0.765	cubic meters	m <sup>3</sup>
NOTE: volumes greater than 1000 L shall be shown in m <sup>3</sup>				
MASS				
oz	ounces	28.35	grams	g
lb	pounds	0.454	kilograms	kg
T	short tons (2000 lb)	0.907	megagrams (or "metric ton")	Mg (or "t")
TEMPERATURE (exact degrees)				
°F	Fahrenheit	5 (F-32)/9 or (F-32)/1.8	Celsius	°C
ILLUMINATION				
fc	foot-candles	10.76	lux	lx
fl	foot-Lamberts	3.426	candela/m <sup>2</sup>	cd/m <sup>2</sup>
FORCE and PRESSURE or STRESS				
lbf	poundforce	4.45	newtons	N
lbf/in <sup>2</sup>	poundforce per square inch	6.89	kilopascals	kPa

APPROXIMATE CONVERSIONS TO SI UNITS				
SYMBOL	WHEN YOU KNOW	MULTIPLY BY	TO FIND	SYMBOL
<b>LENGTH</b>				
in	inches	25.4	millimeters	mm
ft	feet	0.305	meters	m
yd	yards	0.914	meters	m
mi	miles	1.61	kilometers	km
<b>AREA</b>				
in <sup>2</sup>	square inches	645.2	square millimeters	mm <sup>2</sup>
ft <sup>2</sup>	square feet	0.093	square meters	m <sup>2</sup>
yd <sup>2</sup>	square yard	0.836	square meters	m <sup>2</sup>
ac	acres	0.405	hectares	ha
mi <sup>2</sup>	square miles	2.59	square kilometers	km <sup>2</sup>
<b>VOLUME</b>				
fl oz	fluid ounces	29.57	milliliters	mL
gal	gallons	3.785	liters	L
ft <sup>3</sup>	cubic feet	0.028	cubic meters	m <sup>3</sup>
yd <sup>3</sup>	cubic yards	0.765	cubic meters	m <sup>3</sup>
NOTE: volumes greater than 1000 L shall be shown in m <sup>3</sup>				
<b>MASS</b>				
oz	ounces	28.35	grams	g
lb	pounds	0.454	kilograms	kg
T	short tons (2000 lb)	0.907	megagrams (or "metric ton")	Mg (or "t")
<b>TEMPERATURE (exact degrees)</b>				
°F	Fahrenheit	5 (F-32)/9 or (F-32)/1.8	Celsius	°C
<b>ILLUMINATION</b>				
fc	foot-candles	10.76	lux	lx
fl	foot-Lamberts	3.426	candela/m <sup>2</sup>	cd/m <sup>2</sup>
<b>FORCE and PRESSURE or STRESS</b>				
lbf	poundforce	4.45	newtons	N
lbf/in <sup>2</sup>	poundforce per square inch	6.89	kilopascals	kPa

\*SI is the symbol for the International System of Units. Appropriate rounding should be made to comply with Section 4 of ASTM E380.

# TABLE OF CONTENTS

SI* (MODERN METRIC) CONVERSION FACTORS.....	iv
<b>CHAPTER 1 - INTRODUCTION.....</b>	<b>1</b>
<b>CHAPTER 2 - THE IMPACT OF DIFFERENT RELATIVE HUMIDITIES ON CURLING.....</b>	<b>3</b>
2.1 INTRODUCTION.....	3
2.2 EXPERIMENTAL INVESTIGATIONS.....	3
<b>2.2.1 Materials.....</b>	<b>3</b>
<b>2.2.2 Mixture Proportions and Procedures.....</b>	<b>4</b>
<b>2.2.3 Sample Preparation, Casting and Curing.....</b>	<b>5</b>
<b>2.2.4 Test Procedure and Measurement.....</b>	<b>8</b>
2.3 RESULTS AND DISCUSSION.....	10
<b>2.3.1 Paste Beams.....</b>	<b>10</b>
<b>2.3.2 Concrete Beams.....</b>	<b>13</b>
2.4 CONCLUSIONS.....	17
<b>CHAPTER 3 - THE IMPACT OF DIFFERENT CURING METHODS ON CURLING IN FIELD CONDITIONS.....</b>	<b>19</b>
3.1 INTRODUCTION.....	19
3.2 EXPERIMENTAL INVESTIGATIONS.....	20
<b>3.2.1 Materials.....</b>	<b>20</b>
<b>3.2.2 Mixture Proportions and Procedures.....</b>	<b>20</b>
<b>3.2.3 Sample Preparation, Casting and Curing.....</b>	<b>21</b>
3.3 TEST PROCEDURE AND MEASUREMENT.....	23
3.4 RESULTS.....	24
3.5 DISCUSSION.....	33
<b>3.5.1 Weather Condition in the Field.....</b>	<b>33</b>
<b>3.5.2 Mass Change.....</b>	<b>33</b>
<b>3.5.3 Relative Humidity Change.....</b>	<b>35</b>
<b>3.5.4 Strain Change.....</b>	<b>36</b>
3.6 CONCLUSION.....	36
<b>CHAPTER 4 – INSTRUMENTATION OF I-44 AND LEWIS.....</b>	<b>38</b>
<b>4.1 INTRODUCTION.....</b>	<b>38</b>

<b>4.2 INSTRUMENTATION .....</b>	<b>38</b>
4.3 APPLICATION OF THE CURING METHODS.....	43
4.4 RESULTS AND DISCUSSION .....	45
4.5 CONCLUSION .....	54
<b>CHAPTER 5 - SENSITIVITY ANALYSIS OF DARWIN-ME TO BASE FRICTION... 55</b>	
5.1 INTRODUCTION.....	55
5.2 DISCUSSION.....	57
<b>5.2.1 CRCP .....</b>	<b>57</b>
<b>5.2.2 JPCP .....</b>	<b>60</b>
5.3 SUMMARY.....	64
6.1 Investigation of Oklahoma CRCP .....	65
6.2 Investigation of LTPP database sites .....	67
<b>CHAPTER 7 - A COMPARRISON BETWEEN FIELD INVESTIGATION AND PREDICTED PERFORMANCE FROM DARWIN-ME .....</b>	<b>70</b>
7.1 Coefficient of Thermal Expansion.....	70
7.2 Shrinkage.....	71
<b>CHAPTER 8 - CONCLUSIONS.....</b>	<b>74</b>



# LIST OF FIGURES

Figure 1 - An overview of the paste sample investigated.....	5
Figure 2 - An overview of the concrete sample investigated for this testing.....	8
Figure 3 - Comparison between the mass loss of the paste beams over the time .....	10
Figure 4 - Comparison between the maximum curling of paste beams.....	11
Figure 5 - Comparison between the mass changes of concrete beams in 40% vs. 70% RHs .....	13
Figure 6 - Comparison between the RH profiles in 40% vs. 70% RH. ....	14
Figure 7 - Comparison between the shrinkage profiles in 40% vs. 70% RH. ....	15
Figure 8 - Comparison between the shrinkage profiles in 40% vs. 70% RH .....	16
Figure 9 - An overview of the sample investigated for this testing .....	22
Figure 10 - The minimum, maximum, and average temperature for each month.....	25
Figure 11 - Precipitation and the minimum, maximum, and average RH .....	26
Figure 12 - The mass change of the concrete specimens and rainfall events at the exposure site .....	27
Figure 13 - The average RH at the depth 0.525” and the rainfall events .....	29
Figure 14 - Average RH profiles for different curing methods.....	30
Figure 15 - Strain at a depth of 0.525” of the concrete after being exposed.....	31
Figure 16 - Average strain profiles for different curing methods .....	33
Figure 17 - Casting the concrete pavement.....	38
Figure 18 - Curing materials and methods used on the pavement .....	39
Figure 19 - A strain gage tied to the steel bars .....	40
Figure 20 - RH sensors glued to rods .....	41
Figure 21 - Top view of a typical slab to show the coordination of all the gages.....	42
Figure 22 - The strain gage locations for each curing method .....	43
Figure 23 - The water-wax based curing compound applied by the contractor approximately 30 minutes after paving .....	44
Figure 24 - PAMS curing compound applied by the research team .....	44
Figure 25 - Wet curing for five days under white plastic sheets.....	44

Figure 26 - Temperature profiles for location 1 at 0.1, 30, and 100 days after paving.....	46
Figure 27 - Temperature profiles for location 2 at 0.1, 30, and 100 days after paving.....	47
Figure 28 - Temperature profiles for location 3 at 0.1, 30, and 100 days after paving.....	48
Figure 29 - Strain profiles for location 1 at 0.1, 30, and 100 days after paving.....	50
Figure 30 - Strain profiles for location 2 at 0.1, 30, and 100 days after paving.....	51
Figure 31 - Strain profiles for location 3 at 0.1, 30, and 100 days after paving.....	52
Figure 32 – RH over the time for location B at different depths .....	54
Figure 33 - Terminal IRI vs. friction coefficient for CRCP with subgrade resilient modulus .....	58
Figure 34 - CRCP punchout vs. friction coefficient with subgrade resilient modulus of 8,000 psi .....	58
Figure 35 - Terminal IRI vs. friction coefficient for CRCP with different subgrade stiffness.....	59
Figure 36 - CRCP Punchout vs. friction coefficient with different subgrade stiffness .....	59
Figure 37 - Terminal IRI vs. friction loss for JPCP with subgrade resilient modulus of 8000 psi.....	60
Figure 38 - Transverse cracking vs. friction loss for JPCP with subgrade resilient modulus of 8000 psi .....	61
Figure 39 - Terminal IRI vs. friction loss for JPCP with different subgrade stiffness.....	62
Figure 40 - Transverse cracking vs. friction loss for JPCP with different subgrade stiffness .....	63
Figure 41 - The CTE value for concrete mixtures with different amounts of coarse aggregate. ....	71
Figure 42 - The expansion is shown over time for samples with different cement contents. A negative expansion means that the sample is shrinking. ....	72
Figure 43 - The weight loss of the samples over time when stored in a 40% relative humidity room. ....	72

# LIST OF TABLES

Table 1 - Oxide analysis of the cement used for paste beams .....	3
Table 2 - The oxide analysis of the cement used in the concrete.....	4
Table 3 - The oxide analysis of the fly ash used in the concrete.....	4
Table 4 - The mixture proportions used in this experiment (lb/yd <sup>3</sup> ) .....	5
Table 5 - The oxide analysis of the cement and the phase concentrations from Bogue equations.....	20
Table 6 - The oxide analysis of the fly ash used in the testing.....	20
Table 7 - The mixture proportions used in this experiment (lb/yd <sup>3</sup> ) .....	21
Table 8 - All curing methods used before the exposure .....	23
Table 9 - The surface of cured samples with different curing compounds after 100 and 190 days ....	28
Table 10 - CRCP Sections.....	56
Table 11 - JPCP Sections.....	56
Table 12 - Baseline Design Values.....	57
Table 13 - Summary of the CRCP pavements investigated.....	66
Table 14 - The table shows a comparison to the punchouts measured and those predicted by Darwin-ME .....	67
Table 15 - Inputs for Darwin-ME for Oklahoma concrete LTPP sites.....	68

# CHAPTER 1 - INTRODUCTION

This document provides an update on the ODOT Project “Development and Implementation of the MEPDG for Oklahoma – Phase II”. This work focuses primarily on the field instrumentation of I-44 in Tulsa, Oklahoma as well as some field measurements of specimens with different curing methods. Results are also shown for a sensitivity analysis of Darwin-ME of different base friction and stiffness and for the performance of LTPP sites in Oklahoma. A short summary is also given of each task on the project and an overview of the progress to date is included.

## Task A – Obtain data from LTPP sites in Oklahoma

The research team is planning on visiting different sites in Oklahoma that were used to create the LTPP database that is used by Darwin-ME. On these visits the research team will be able to measure the distress in the field and compare with the values reported by FHWA and other reports.

## Task B – Compare obtained LTPP data to predicted values

In this task the research team will compare the measured values obtained from the LTPP sites and compare them to the values predicted by Darwin-ME. A comparison of the performance of CRCP pavements in the state will also be made to the predicted Darwin-ME values.

## Task C – Investigate the adjustment of local calibration factors

Based on the findings in Task A and B suggestions will be made about the accuracy of the Darwin-ME for different failure modes and adjustments will be made to Darwin-ME.

Task D – Investigate the impact of different curing methods on curling and warping of concrete pavements

The research team has instrumented a CRCP on I-44 in Tulsa. Four different curing methods were used on the pavements and their performance was monitored with internal strain, relative humidity, and external temperature and relative humidity measurements. In addition a number of samples were stored outside and the strain, relative humidity, and weight change was measured. These samples will serve as great companion samples to those measured in the field. Work is also presented on the curling of specimens stored at 65% relative humidity.

Task E – Characterizing pavement mixtures

In this measurement some changes to the recommended values of the Darwin-ME. Specifically the research team is measuring the impact of different aggregates on the ultimate drying shrinkage, the change in the coefficient of thermal expansion caused by using optimized graded concrete, and the impact on strength values for optimized graded concrete. These recommendations will provide helpful inputs for ODOT on their future design values.

# CHAPTER 2 - THE IMPACT OF DIFFERENT RELATIVE HUMIDITIES ON CURLING

## 2.1 INTRODUCTION

This work examines the curling of cement and concrete samples caused by differential drying in laboratory conditions that are close to the average relative humidity (RH) in Oklahoma. Previous work in phase I of this project showed that in 40% RH drying conditions the magnitude of curling increased with the duration of wet curing. These findings provide guidance for wet curing durations for slabs that must be resistant to volume change in different drying conditions.

## 2.2 EXPERIMENTAL INVESTIGATIONS

### 2.2.1 Materials

The Portland cement used for paste beams meets the requirements of both a type I and II cement, according to ASTM C150 and AASHTO M85. The oxide analysis and the estimated phases are given in **Table 1**.

**Table 1 - Oxide analysis of the cement used for paste beams**

chemical test results (%)					
SiO <sub>2</sub>	Al <sub>2</sub> O <sub>3</sub>	MgO	Fe <sub>2</sub> O <sub>3</sub>	CaO	SO <sub>3</sub>
20.23	4.77	1.90	3.23	64.15	2.52
phase concentrations (%)					blaine
C <sub>3</sub> S	C <sub>2</sub> S	C <sub>3</sub> A	C <sub>4</sub> AF	(cm <sup>2</sup> /g)	
63.56	10.05	7.18	9.83	3713	

The cement used for concrete samples is type I, according to ASTM C150, and its chemical analysis is shown in the **Table 2**. Samples were made with dolomitic limestone aggregate and natural river sand used commercially in concrete.

**Table 2 - The oxide analysis of the cement used in the concrete**

chemical test results (%)					
SiO <sub>2</sub>	Al <sub>2</sub> O <sub>3</sub>	MgO	Fe <sub>2</sub> O <sub>3</sub>	CaO	SO <sub>3</sub>
20.77	4.57	2.37	2.62	62.27	3.18
Na <sub>2</sub> O	K <sub>2</sub> O	TiO <sub>2</sub>	P <sub>2</sub> O <sub>5</sub>	SrO	BaO
0.19	0.32	0.34	0.14	0.22	0.07
phase concentrations (%)					
C <sub>3</sub> S	C <sub>2</sub> S	C <sub>3</sub> A	C <sub>4</sub> AF		
52.13	20.22	7.68	7.97		

An ASTM C618 class C fly ash with chemical analysis shown in **Table 3** was also used.

**Table 3 - The oxide analysis of the fly ash used in the concrete**

chemical test results (%)						
K <sub>2</sub> O	BaO	MgO	SrO	CaO	SO <sub>3</sub>	Na <sub>2</sub> O
0.58	0.72	5.55	0.39	23.12	1.27	1.78
SiO <sub>2</sub>	Al <sub>2</sub> O <sub>3</sub>	MnO <sub>2</sub>	P <sub>2</sub> O <sub>5</sub>	Fe <sub>2</sub> O <sub>3</sub>	TiO <sub>2</sub>	
38.71	18.82	0.02	1.46	5.88	1.35	

### 2.2.2 Mixture Proportions and Procedures

For both the paste and concrete beams the mixtures had a water to cement ratio (w/cm) of 0.42. All of the aggregate, both coarse and fine, were brought into the temperature controlled mixing facility at least a day before and their batch weights were corrected based on the moisture content of the aggregates. At mixing the aggregates were charged into the mixer along with approximately two-thirds of the mixing water. The combination was mixed for three minutes. Next any clumped fine aggregate was removed from the walls of the mixer. Then the cement and fly ash is loaded into the mixer, followed by the remaining mixing water. The mixer was turned on for three minutes. Once this mixing period was complete, the mixture was left to “rest” for the following two minutes while the buildup of material along the walls was removed. Next the mixer was allowed to run for three minutes. The slump (ASTM

C143), unit weight (ASTM C138) and the air content (ASTM C231) were measured.

The typical mixture proportion used is presented in **Table 4** for a cubic meter.

**Table 4 - The mixture proportions used in this experiment (lb/yd<sup>3</sup>)**

cement	fly ash	course aggregate	fine aggregate	water
451.2	112.7	1850	1244	231.2

### 2.2.3 Sample Preparation, Casting and Curing

#### 2.2.3.1 Paste beams

The paste mixtures were prepared according to ASTM C305. Three paste beams with dimensions of 39.4"×2.4"×0.5" were consolidated in plastic molds from each mixture. An overview of these beams is shown in **Fig. 1**. This specimen size was chosen so that the sample was thin but had a large surface area. Several others have found that the developed stresses and shrinkage strains due to the moisture gradients during drying is highly related to specimen size (McDonald and Roper 1993; Pickett 1946; Browne 1967). After casting, all specimens were cured with wet burlap on the finished surface for 24 hours at 73 °F and then demolded. This was done to ensure that the sample had some initial strength for handling. After removing the specimens from the molds the samples were sealed with wax on all sides but the finished surface. The wax was used because it is economical and easy to apply.

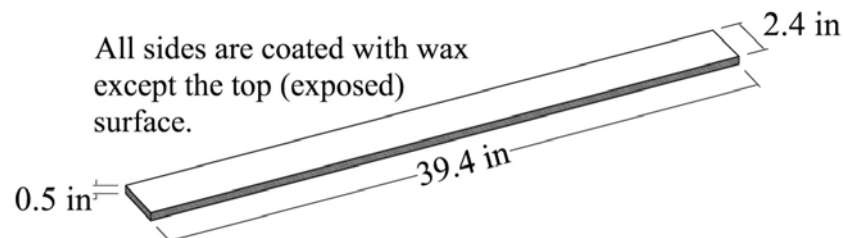


**Figure 1 - An overview of the paste sample investigated**



After demolding the specimens were weighed before and after sealing with wax. The finished surface of the beam was cured for different durations while the beams were stored in a 73 °F and 70% RH environmental chamber. After the specified curing period the curing material was removed from the sample. The sample was then left in the chamber to lose moisture from the unsealed, finished surface.

Since only the top surface of the sample was exposed to the drying environment, this created a moisture gradient in the sample. This gradient caused differential shrinkage strains to occur that caused the specimen to curl. This test is advantageous, as the moisture loss is quick and the resulting gradients can be large. This leads to a significant curling deformation of the specimens that is easy to measure. To ensure that the curling measurements were not impacted by gravity the beams were stored on their sides. This test was modeled after previous work by Berke et al. (2004) to investigate the effectiveness of shrinkage reducing admixtures to minimize curling.

Specimens with different durations of wet curing were compared. Samples were kept in saturated burlap for 1, 3, 7, and 14 days of additional curing after demolding and waxing. The burlap was wetted every day to ensure that it remained saturated. After the curing was removed the specimens were subjected to a 70% RH and 73 °F drying environment within an environmental chamber. Other samples received no curing after demolding. All specimens were stored at 73 °F throughout the testing.

### 2.2.3.2 Concrete beams

The specimens used for this work are a simplified version of much larger beam tests completed by Springenschmid et al. (2001), Hansen et al. (2007), and Hajibabaei (2011). By studying these smaller elements it was possible to investigate a greater number of samples and variables more economically. Also it allowed the weight change to be measured in addition to the strain and RH. This is not possible with the larger beam tests previously investigated.

For this work all drying is assumed to originate from the top surface of the slab. To simulate this, a waterproof membrane is used on all faces of the sample except for the top. An overview of these beams is shown in **Fig. 2**. For this testing all specimens were cast and stored in an environmental chamber at 73 °F and about 70% RH. In this experiment the specimen was 3"×4"×10.25". The moisture barrier was used as a form liner during casting. This material had a plastic waterproof membrane on one side and fibers on the other. The fibers were oriented so that they bonded to the wet concrete and provided a tight fit of the water proof layer on the outside of the beam.

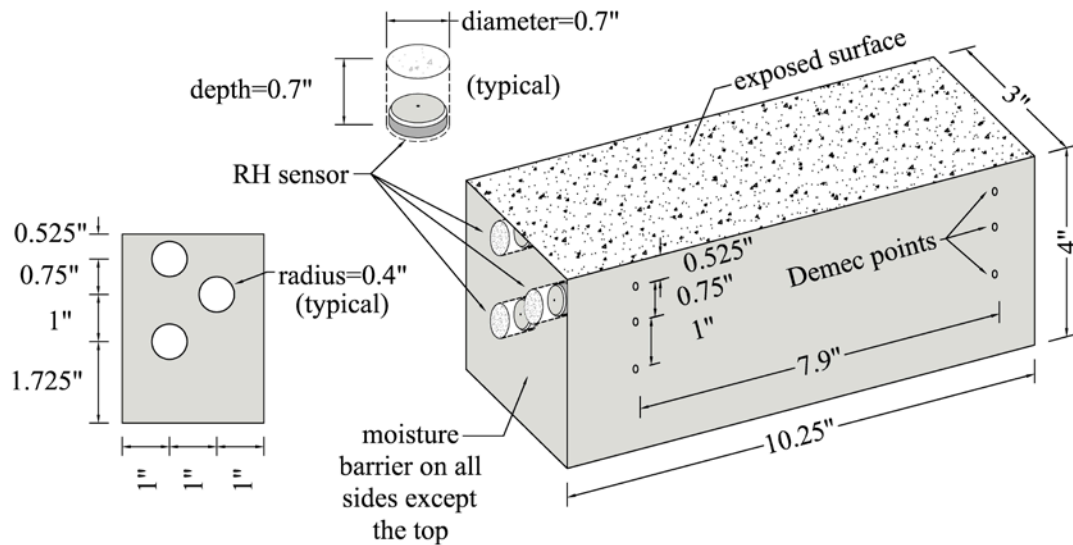


**Figure 2 - An overview of the concrete sample investigated for this testing**

This concrete specimen was carefully demolded 24 hours after casting and the interface between the membrane and the concrete were sealed by wax. Specimens were prepared with no-curing and 7 and 14 days of wet curing with wet burlap and a plastic tarp. While drying the beams were flipped on their side and placed on wooden dowels to minimize the impact of the self-weight on the curling measurements.

## 2.2.4 Test Procedure and Measurement

### 2.2.4.1 Paste beams

To measure the curling, rubber bands were used to hold the ends of the specimen to a flat aluminum plate with the uncoated surface of the specimen facing the plate. The distance between the aluminum plate and the specimen is measured at regular locations along the length with a caliper of 0.0005" accuracy. The curling of the beam is symmetric and the maximum is at the middle of the beam. The loss of moisture of the sample was measured through the weight loss over time with

0.00022 lb accuracy. After finishing the measurements, the specimen is returned to the chamber room until the next measurement.

#### *2.2.4.2 Concrete beams*

The surface strain of the beam was measured at 3 different depths, as shown in **Fig. 2**. Surface mounted stainless steel gage points were glued to the surface of the beams. This was achieved by burning through the membrane in a localized area and then gluing one of these gage points. Each gage point has a machined cone in the surface that fit within a hand held mechanical strain gage. The accuracy of this gage was 4 microstrain.

The RH of the beams was measured at 0.525", 1.275", and 2.275" from the finished surface starting four days after the termination of curing. This was done by using the DS1923 Hygrochron Temperature/Humidity Logger iButtons. The sensors were placed in 0.7" deep holes with 0.7" diameter that were cast into the side of the concrete. During demolding the forms used to make these holes were removed and the holes were covered with tape. These sensors were programmed to take RH measurements every hour. The gages were inserted after four days of curing to prevent failure due to the high amount of moisture in the concrete. After demolding the holes were sealed with water proof tape. This tape was removed briefly when the sensors were added to the beam and each month when the data was obtained from the sensors.

The RH sensors were calibrated according to ASTM E104 with four different salt saturated solutions. The RH calibration range was between 57.6% and 97.3%. This was chosen in order to cover the ranges of humidity expected in the testing. A

specific calibration was generated for each sensor and applied to all subsequent measurements.

## 2.3 RESULTS AND DISCUSSION

### 2.3.1 Paste Beams

The mass loss of the paste samples in 70% RH is shown in **Fig. 3** in comparison with that of the samples in 40%.

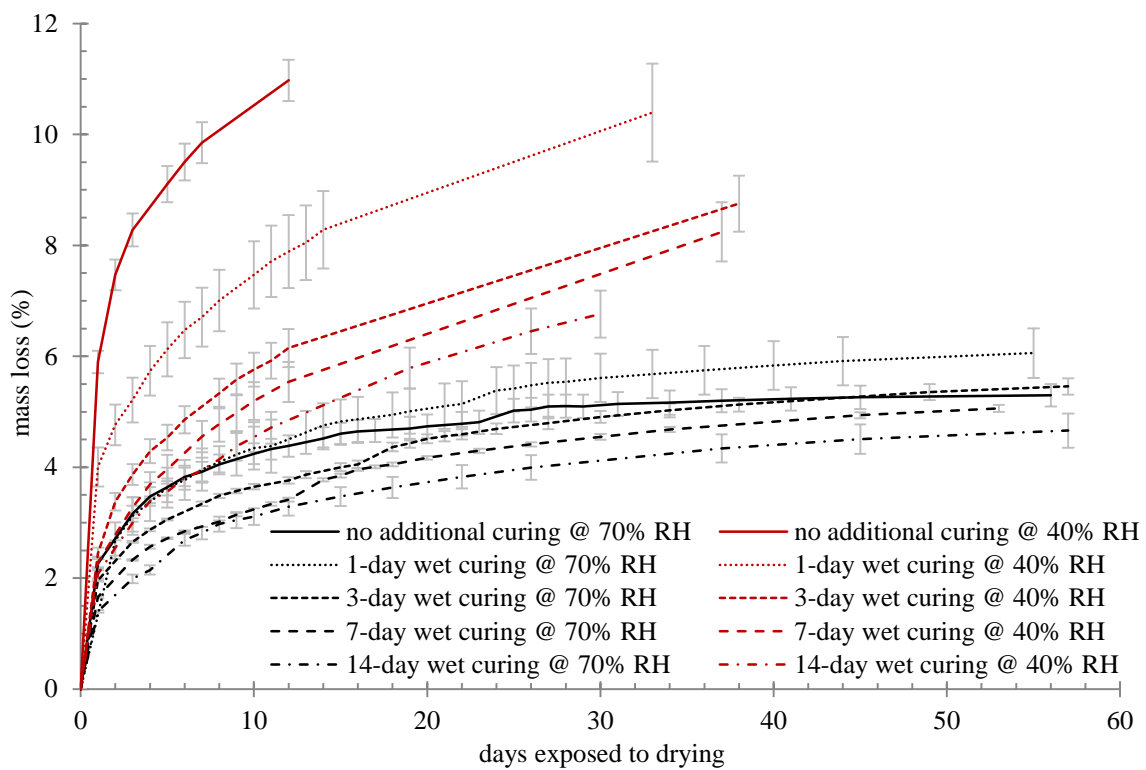


**Figure 3 - Comparison between the mass loss of the paste beams over the time**

As shown above, the mass loss of the paste samples in 40% RH is greater than the samples that were exposed to 70% RH. The maximum mass loss of the no curing at 40% RH is the most and the least mass loss was observed in 14-day wet curing in 70% RH. Also, the difference between the mass losses of different curing

lengths is less in 70% compared to 40% RH's. Also the increase in the curing length has decreased the mass loss amount.

The curling deflection of the paste samples exposed to 70% versus 40% RH's is shown in **Fig. 4**.

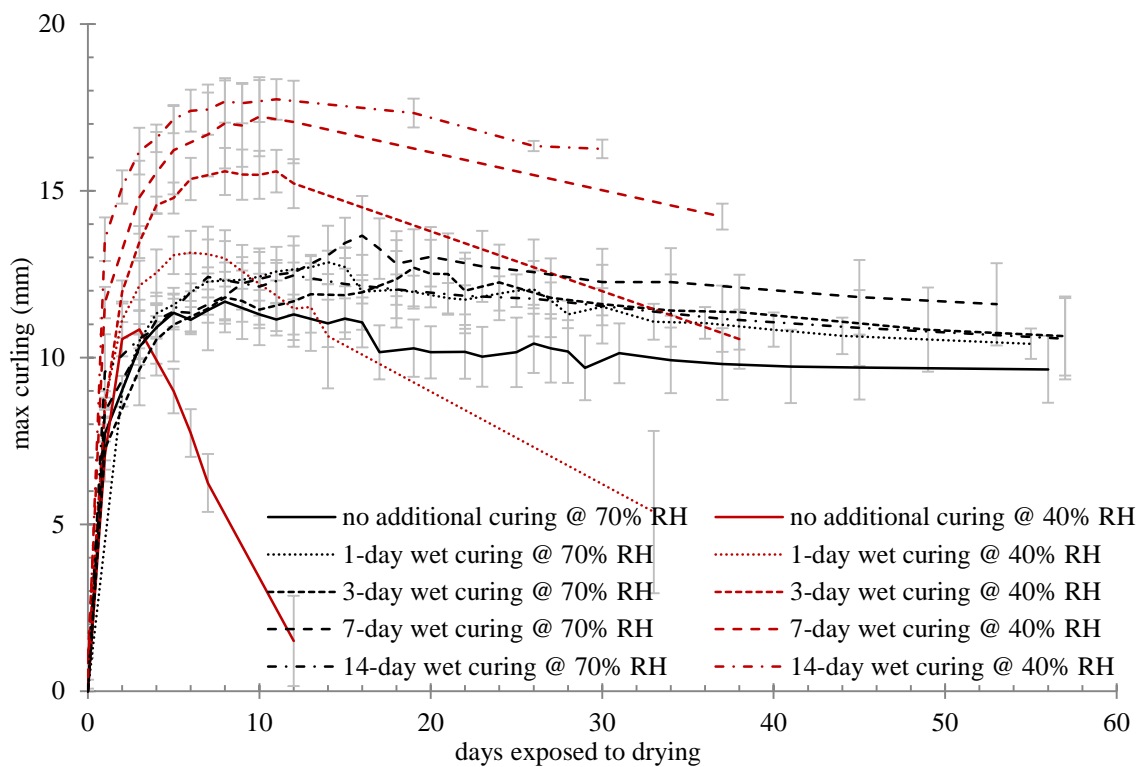


**Figure 4 - Comparison between the maximum curling of paste beams**

As shown in **Fig. 4**, the samples in 70% RH have less curling compared to samples in 40% RH and there is a less difference between the maximum deflections of different curing lengths in the more humid environment compared to deflections in the more extreme drying condition. Also the increase in the length of curing has increased the maximum curling.

This mass loss will continue until the internal RH reaches equilibrium with the environment. However, because the moisture loss at the top and bottom of the sample is different, there is a differential in shrinkage and so the sample curls. With increased drying, the curl decreases as the material in the bottom of the sample begins to shrink and the differential in shrinkage between the top and bottom is reduced.

Additional curing will sustain hydration and decrease the porosity and permeability of cement paste. Because the pore sizes are smaller for materials with a greater degree of hydration, the degree of saturation will be higher at a given RH. This increase in saturation may be explained by the Kelvin-Laplace equation, which describes the minimum pore size emptied at a given RH at equilibrium. This means that curing will cause a higher level of saturation and will increase the effective pressure in the pore network and, therefore, the shrinkage on drying (Coussy et al. 2004).

Also, the decrease in permeability with extended curing makes it more difficult for a specimen to lose moisture from drying. This is why specimens that are cured longer lost moisture at slower rates, and required more time to reach their maximum amount of curling. Moreover, the additional wet curing may increase the water content of the samples, which will increase the length of drying time needed for the samples to reach their maximum curling deflection.

A high storage RH causes a decrease in the shrinkage gradient and the resulting deflection. Also it delays the drying time required to reach the peaks of

deflection as shown above. Moreover, the samples have less mass loss in higher RHs.

### 2.3.2 Concrete Beams

The mass change of the concrete beams in the 40% versus 70% RH is shown in Fig. 5.

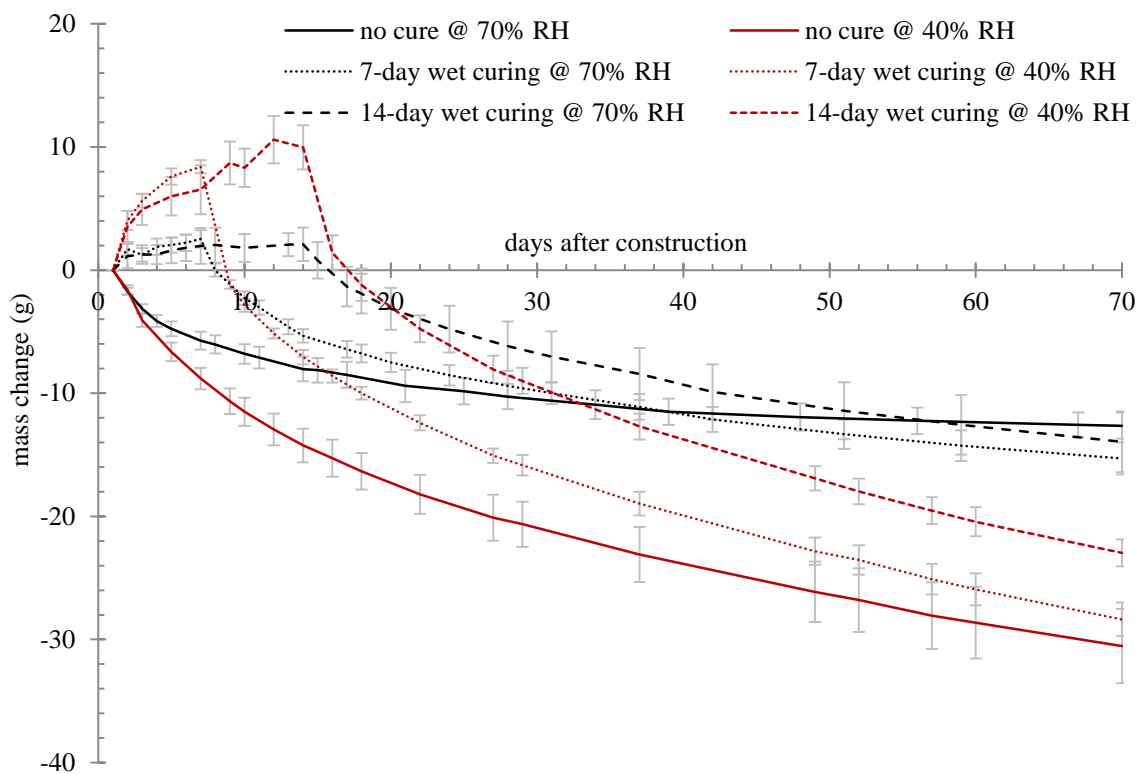


**Figure 5 - Comparison between the mass changes of concrete beams in 40% vs. 70% RHs**

The samples stored in 40% RH have more mass loss and there is a greater mass loss difference between samples when compared to the samples stored in 70% RH. The wet cured samples increased in mass from the additional water that was supplied from wet curing. However, when these specimens were dried they quickly lost the extra mass gained from the wet curing. When comparing the first 3



days of drying, the 7 and 14-day wet cured samples had a greater rate of mass loss than the sample that was not cured.

The RH profiles within the samples for 5, 25, 50, and 200 days after exposure are shown in **Fig. 6**. The RH gradient is larger for samples that were exposed to the more extreme drying condition. Also, with extended drying the RH decreased faster in the 40% RH.

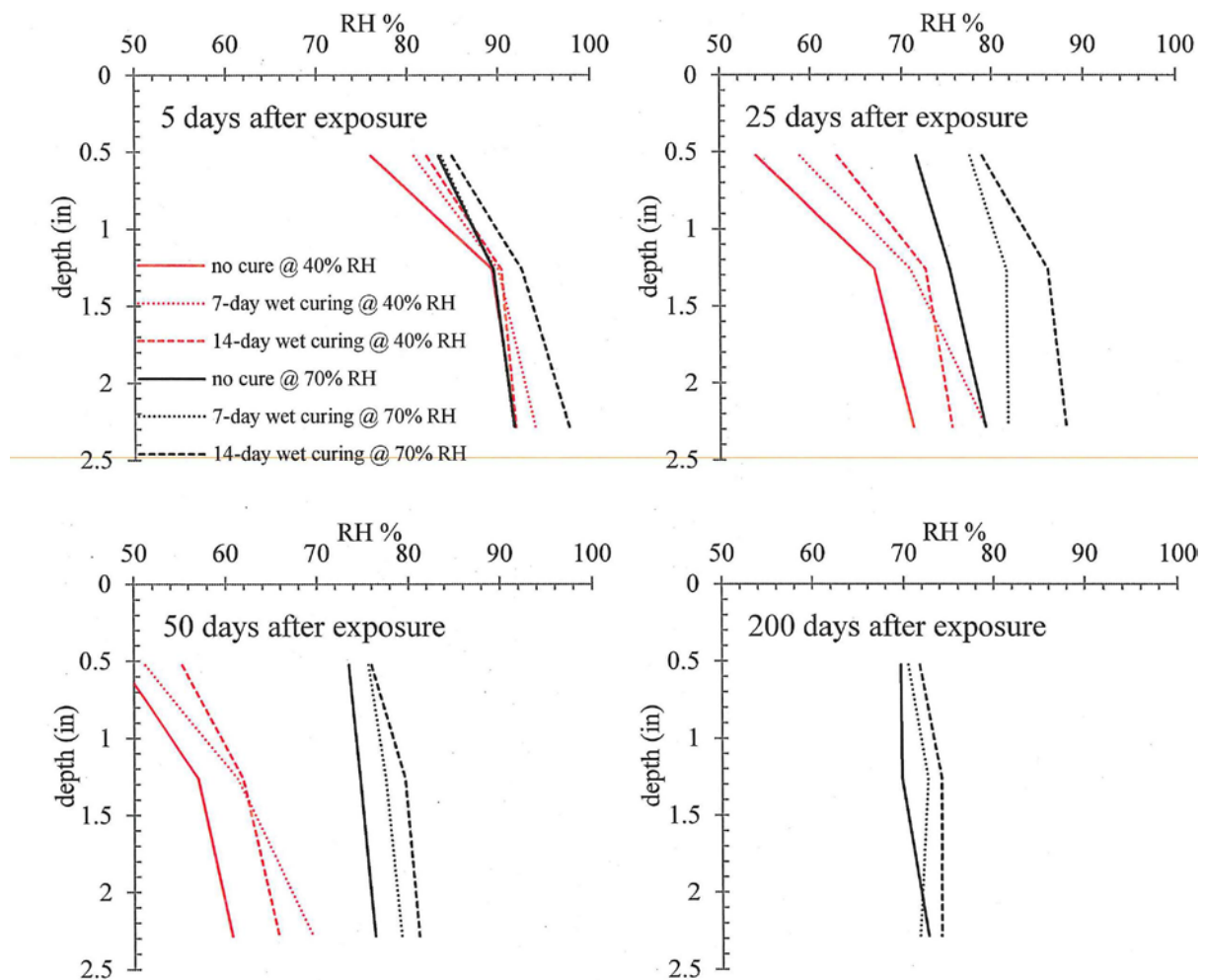


**Figure 6 - Comparison between the RH profiles in 40% vs. 70% RH.**

Using extended wet curing, the samples should have improved levels of hydration and decreased permeability and hence lost less moisture at comparable times. The water loss occurred first on the surface and had not had a major impact on the RH over the depth of the samples. The sample that was not cured showed lower RH at virtually all places in the specimen for all of the compared drying periods.

The shrinkage of the concrete beams at 0.525" depth is shown in **Fig. 7** for 40% versus 70% RH. The shrinkage of the samples in 40% RH is greater and as the curing length was increased then so did the amount of shrinkage that occurred. The rate of shrinkage is greater during the initial drying for the 40% RH samples when compared to the 70% RH.

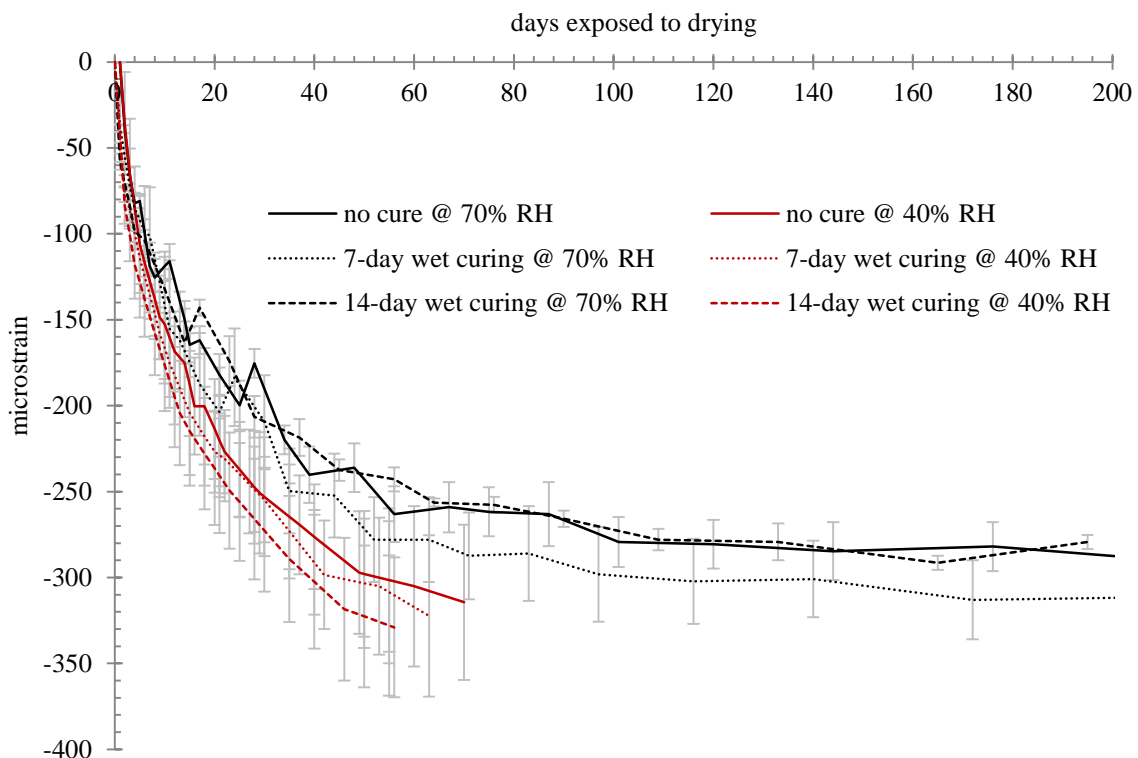


**Figure 7 - Comparison between the shrinkage profiles in 40% vs. 70% RH.**

The shrinkage profiles within the samples for 5, 25, 50, and 200 days after exposure are shown in **Fig. 8**. The shrinkage gradient is larger for samples that were exposed to 40% RH. Also, samples exposed to 40% RH showed greater amounts of shrinkage.

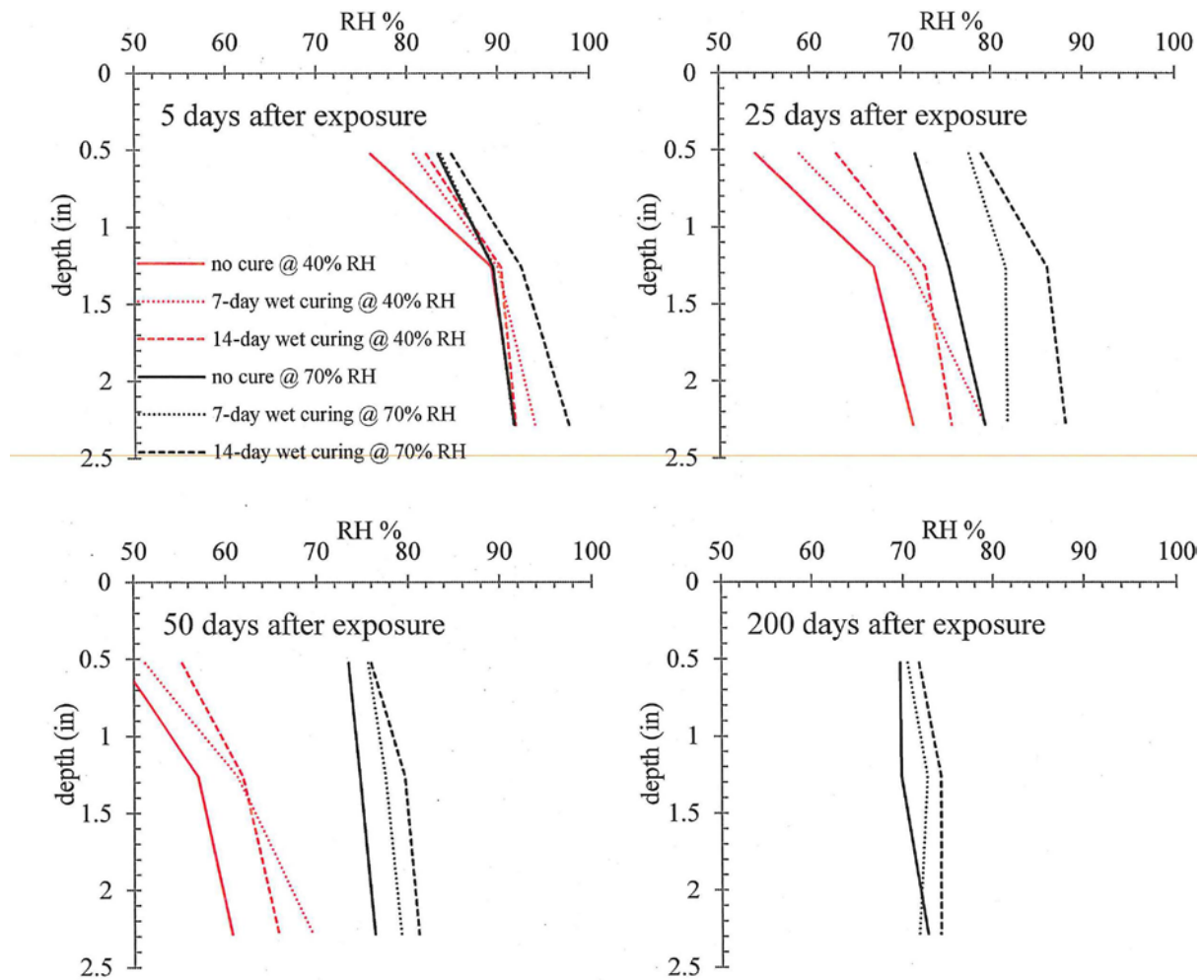


**Figure 8 - Comparison between the shrinkage profiles in 40% vs. 70% RH**

Despite the internal RH being lower for samples with no curing, these samples showed an equal or lower shrinkage strain than the sample with wet curing. This increase in the internal strain gradient is expected to produce a greater amount of curling in the specimen.

It is expected that the permeability of the wet cured specimens is less than that of no cured samples due to the decrease in connectivity and the sizes of the pores from the increased degree of hydration caused by the curing. Also, since these pores are smaller this will lead to an increase in the degree of saturation. As seen before for paste beams, this increase in saturation will increase the effective pressure in the pore network and the drying shrinkage (Coussy et al. 2004). Despite all of these changes occurring in the paste, the shrinkage in the concrete is related to shrinkage in the paste (Picket 1956).

## **2.4 CONCLUSIONS**

Several useful conclusive remarks need to be mentioned from the comparison investigated in this testing:

- Increasing the wet curing length increases the degree of saturation of the paste.
- This increased level of saturation will lead to increased strains on subsequent drying.
- Wet curing will also reduce mass transport.
- This will in turn lead to larger moisture gradients in the sample.
- All of this causes greater curling in wet cured paste and concrete samples.
- The models in Darwin-ME need to be modified.
- If volume change is important for your concrete slab/pavement then it may be beneficial to limit the extent of wet curing.
- In a less severe environment, such as 70% RH, the same trends have been observed but the magnitudes were smaller.

This means that if concrete is going to be used in dry conditions (~ 40% RH), then wet curing can lead to greater volume changes in the structure on drying. However, if the concrete is to be used in a moist environment such as present in Oklahoma (~ 70% RH) then wet curing appears to have minimal impact on the volume change from drying. This means that wet curing shouldn't lead to increased volume change from drying and that it behaves similarly to no curing in curling experiments.

# **CHAPTER 3 - THE IMPACT OF DIFFERENT CURING METHODS ON CURLING IN FIELD CONDITIONS**

## **3.1 INTRODUCTION**

Past research on phase I of this project investigated the curling from differential drying of concrete and the impact on concrete pavements. The research in Chapter 2 used laboratory specimens that were cast and stored in 40% and 70% RH and showed that when a specimen was wet cured then this caused an increase in the amount of curling when it dried. The mechanism for this behavior was attributed to the increased curing leading to a decrease in the pore sizes. On drying the capillary suction in these smaller pores causes increased shrinkage which in turn leads to increased curling. Different curing compounds were also investigated at a number of different coverage rates in Phase I. This work showed that the poly-alpha-methylstyrene (PAMS) performed the best of the curing compounds. Next the resin based and finally the water based performed the worst. Performance with different coverage rates was also investigated.

The work in this report is focused on evaluating the performance of these same specimens in the field and then measuring the shrinkage, weight loss, and RH of the sample. One challenge with this work is that since these samples were stored in the field that the temperature, moisture, and wind varied over time. This means that all of these variables had to be measured while simultaneously measuring the response of the samples. However, these exposure conditions led to a more realistic environmental condition for field concrete.

## 3.2 EXPERIMENTAL INVESTIGATIONS

### 3.2.1 Materials

The cement used in this test is type I, according to ASTM C150, and its chemical analysis is shown in the **Table 5**.

**Table 5 - The oxide analysis of the cement and the phase concentrations from Bogue equations**

chemical test results (%)					
SiO <sub>2</sub>	Al <sub>2</sub> O <sub>3</sub>	MgO	Fe <sub>2</sub> O <sub>3</sub>	CaO	SO <sub>3</sub>
20.77	4.57	2.37	2.62	62.27	3.18
Na <sub>2</sub> O	K <sub>2</sub> O	TiO <sub>2</sub>	P <sub>2</sub> O <sub>5</sub>	SrO	BaO
0.19	0.32	0.34	0.14	0.22	0.07
phase concentrations (%)					
C <sub>3</sub> S	C <sub>2</sub> S	C <sub>3</sub> A	C <sub>4</sub> AF		
52.13	20.22	7.68	7.97		

Samples were made with dolomitic limestone aggregate and natural river sand used commercially in concrete. An ASTM C618 class C fly ash with chemical analysis shown in **Table 6** was also used.

**Table 6 - The oxide analysis of the fly ash used in the testing**

chemical test results (%)						
K <sub>2</sub> O	BaO	MgO	SrO	CaO	SO <sub>3</sub>	Na <sub>2</sub> O
0.58	0.72	5.55	0.39	23.12	1.27	1.78
SiO <sub>2</sub>	Al <sub>2</sub> O <sub>3</sub>	MnO <sub>2</sub>	P <sub>2</sub> O <sub>5</sub>	Fe <sub>2</sub> O <sub>3</sub>	TiO <sub>2</sub>	
38.71	18.82	0.02	1.46	5.88	1.35	

### 3.2.2 Mixture Proportions and Procedures

In the mixtures investigated a w/cm of 0.42 was used. All of the aggregate, both coarse and fine, were brought into the temperature controlled mixing facility at least a day before and their batch weights were corrected for the moisture content.

At mixing the aggregates were charged into the mixer along with approximately two-thirds of the mixing water. The combination was mixed for three minutes. Next any clumped fine aggregate was removed from the walls of the mixer. Then the cement and fly ash is loaded into the mixer, followed by the remaining mixing water. The mixer was turned on for three minutes. Once this mixing period was complete, the mixture was left to “rest” for the following two minutes while the buildup of material along the walls was removed. Next the mixer was allowed to run for three minutes. The slump (ASTM C143), unit weight (ASTM C138) and the air content (ASTM C231) were measured. The typical mixture proportion used is presented in **Table 7** for a cubic yard.

**Table 7 - The mixture proportions used in this experiment (lb/yd<sup>3</sup>)**

cement	fly ash	course aggregate	fine aggregate	water
451.2	112.7	1850	1244	231.2

### 3.2.3 Sample Preparation, Casting and Curing

The specimens used for this work are a simplified version of much larger beam tests completed by Hansen et al. (2007), Springenschmid et al. (2001), and Hajibabae (2011). By studying these smaller elements it was possible to investigate a greater number of samples and variables more economically. Also it allowed the weight change to be measured in addition to the strain and RH. This is not possible with the larger beam tests previously investigated.

For this work all drying is assumed to originate from the top surface of the slab. To simulate this, a waterproof membrane is used on all faces of the sample except for the top. An overview of these beams is shown in **Fig. 9**.



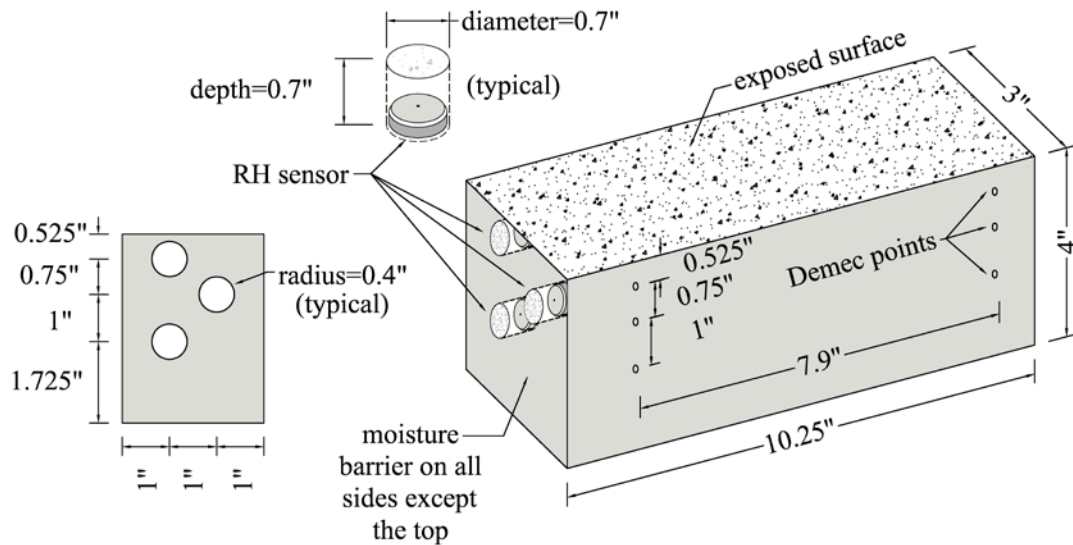


**Figure 9 - An overview of the concrete sample investigated for this testing**

For this testing all specimens were moved after casting to the Oklahoma State University exposure site. This is an area just north of the OSU campus. In this experiment the specimen was 3"×4"×10.25" as outlined in **Fig. 9**. The moisture barrier was used as a form liner during casting. This material had a plastic waterproof membrane on one side and fibers on the other. The fibers were oriented so that they bonded to the wet concrete and provided a tight fit of the water proof layer on the outside of the beam.

This specimen was carefully demolded one day after casting and the interface between the membrane and the concrete was sealed by wax. Specimens were prepared with no-curing, 1, 3, and 7 days of wet curing with wet burlap and a plastic tarp, as well as a number of different curing compound combinations. All curing methods have been summarized in **Table 8**.

**Table 8 - All curing methods used before the exposure**

Name		Curing methods	
1-day wet		Wet curing with wet burlap for 1 day	
3-day wet		Wet curing with wet burlap for 3 days	
7-day wet		Wet curing with wet burlap for 7 days	
No curing		Exposed to the site without any curing	
Sealed		Sealed with wax and wrapped in plastic before exposure to the site	
Water-wax, S 100%	Single layer	water-wax based curing compound	0.04 lbs/ft <sup>2</sup>
Water-wax, S 150%	Single layer	water-wax based curing compound	0.06 lbs/ft <sup>2</sup>
Water-wax, D 100%	Double layer	water-wax based curing compound	0.04 lbs/ft <sup>2</sup> *
Resin, S 100%	Single layer	resin based curing compound	0.04 lbs/ft <sup>2</sup>
PAMS, S 100%	Single layer	poly-alphamethylstyrene curing compound	0.04 lbs/ft <sup>2</sup>

\*The double layer of curing compound was applied in two equal layers of 0.02 lbs/ft<sup>2</sup> for each one for a total coverage of 0.04 lbs/ft<sup>2</sup>.

### 3.3 TEST PROCEDURE AND MEASUREMENT

The surface strain of the beam was measured at 3 different depths, as shown in **Fig. 9**. Surface mounted stainless steel gage points were glued to the surface of the beams. This was achieved by burning through the membrane in a localized area and then gluing one of these gage points. Each gage point has a machined cone in the surface that fit within a hand held mechanical strain gage. The accuracy of this gage was 4 microstrain.

The RH of the beams was measured at 0.525", 1.275", and 2.275" from the finished surface starting four days after the termination of curing. This was done by using the DS1923 Hygrochron Temperature/Humidity Logger iButtons. The sensors were placed in 0.7" deep holes with 0.7" diameter that were cast into the side of the concrete for one sample of each curing method. During demolding the forms used to make these holes were removed and the holes were covered with tape. These sensors were programmed to take RH measurements every hour. The gages were inserted after four days of curing to prevent failure due to the high amount of moisture in the concrete. After demolding the holes were sealed with water proof

tape. This tape was removed briefly when the sensors were added to the beam and each month when the data was obtained from the sensors.

The RH sensors were calibrated according to ASTM E104 “Standard Practice for Maintaining Constant RH by Means of Aqueous Solutions” with four different salt saturated solutions. The RH calibration range was between 57.6% and 97.3%. This was chosen in order to cover the ranges of humidity expected in the testing. A specific calibration was generated for each sensor and applied to all subsequent measurements.

A weather station has been used to measure the wind speed, rainfall, temperature, solar radiation, and RH during the test. These measurements were taken every five minutes.

### **3.4 RESULTS**

**Figure 10** shows the monthly average temperature for the last 5 years in Oklahoma City. The average values were calculated using the daily max, min, and average temperature and RH data collected from weather website wunderground.

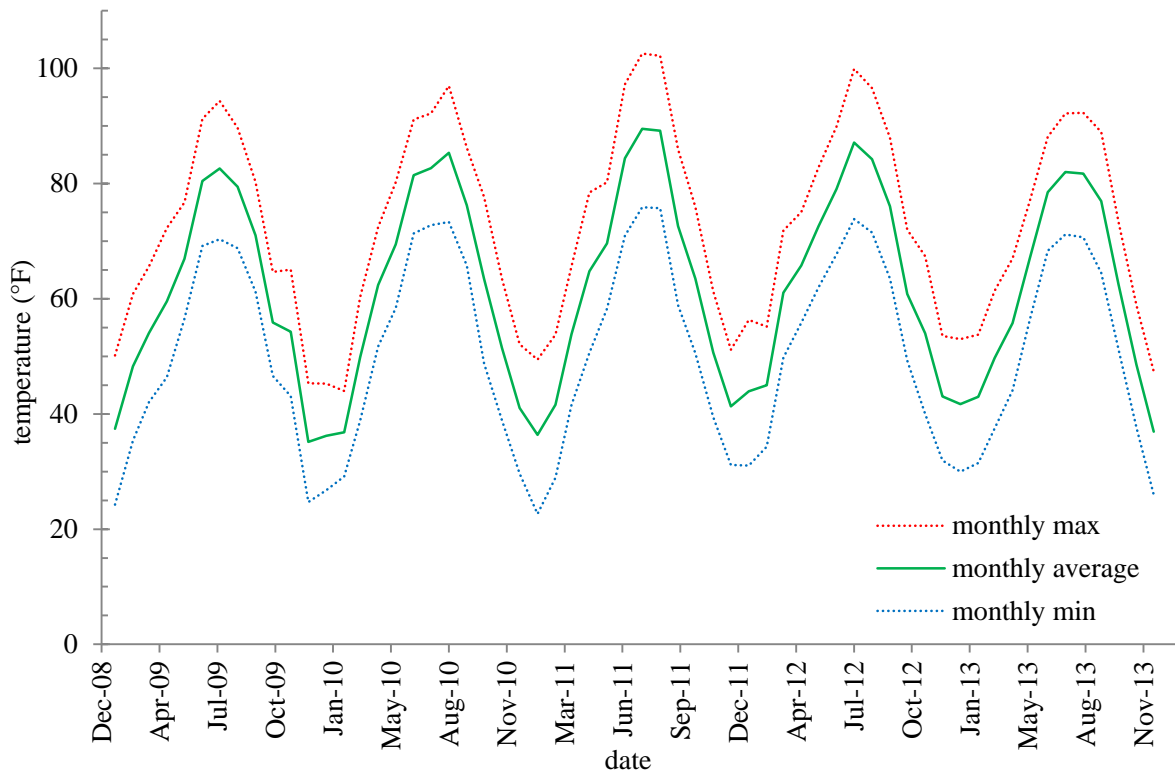


**Figure 10 - The minimum, maximum, and average temperature for each month**

**Figure 11** shows the monthly average RH for the last 5 years in Oklahoma City. The average values were calculated using the daily average RH data collected from weather website wunderground. The running average was calculated for every 30 days. The precipitation has been shown as well.

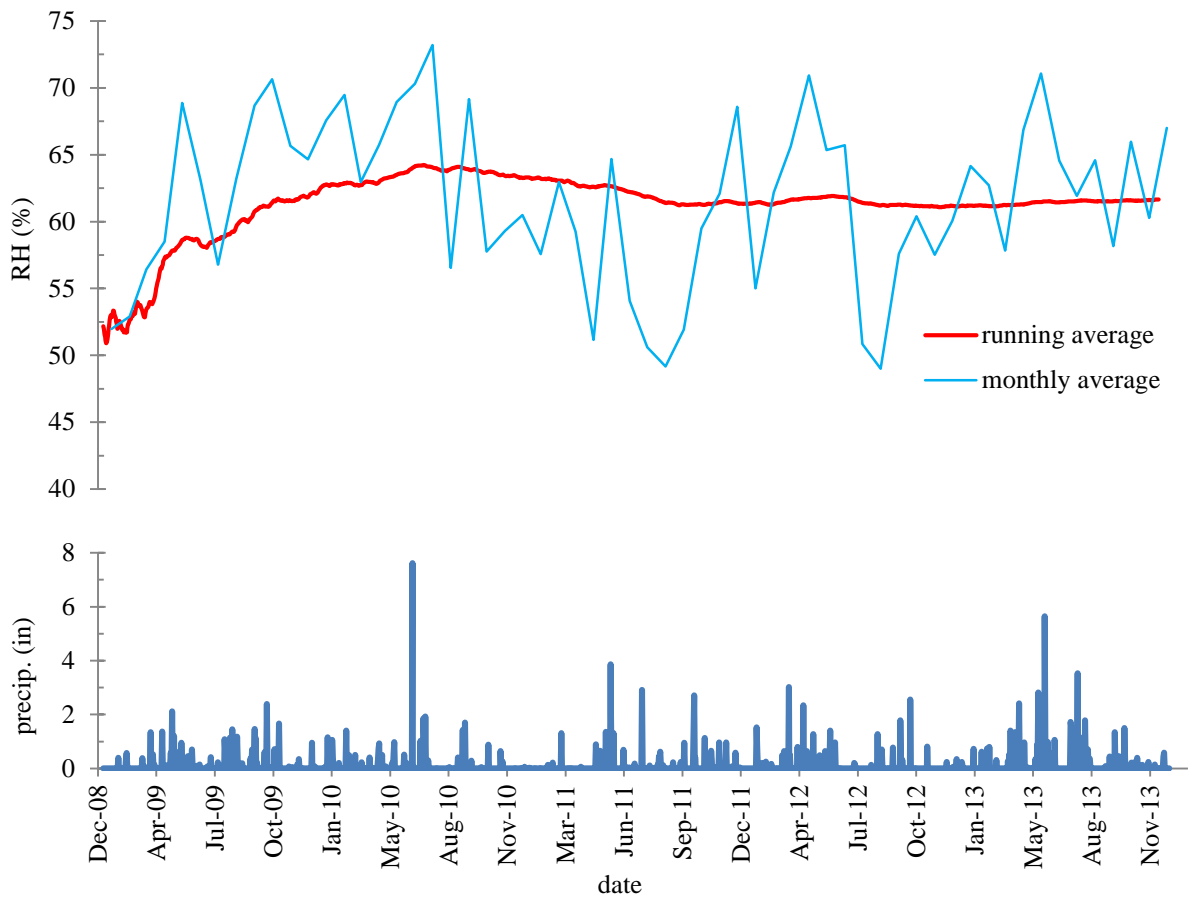


**Figure 11 - Precipitation and the monthly and average RH**



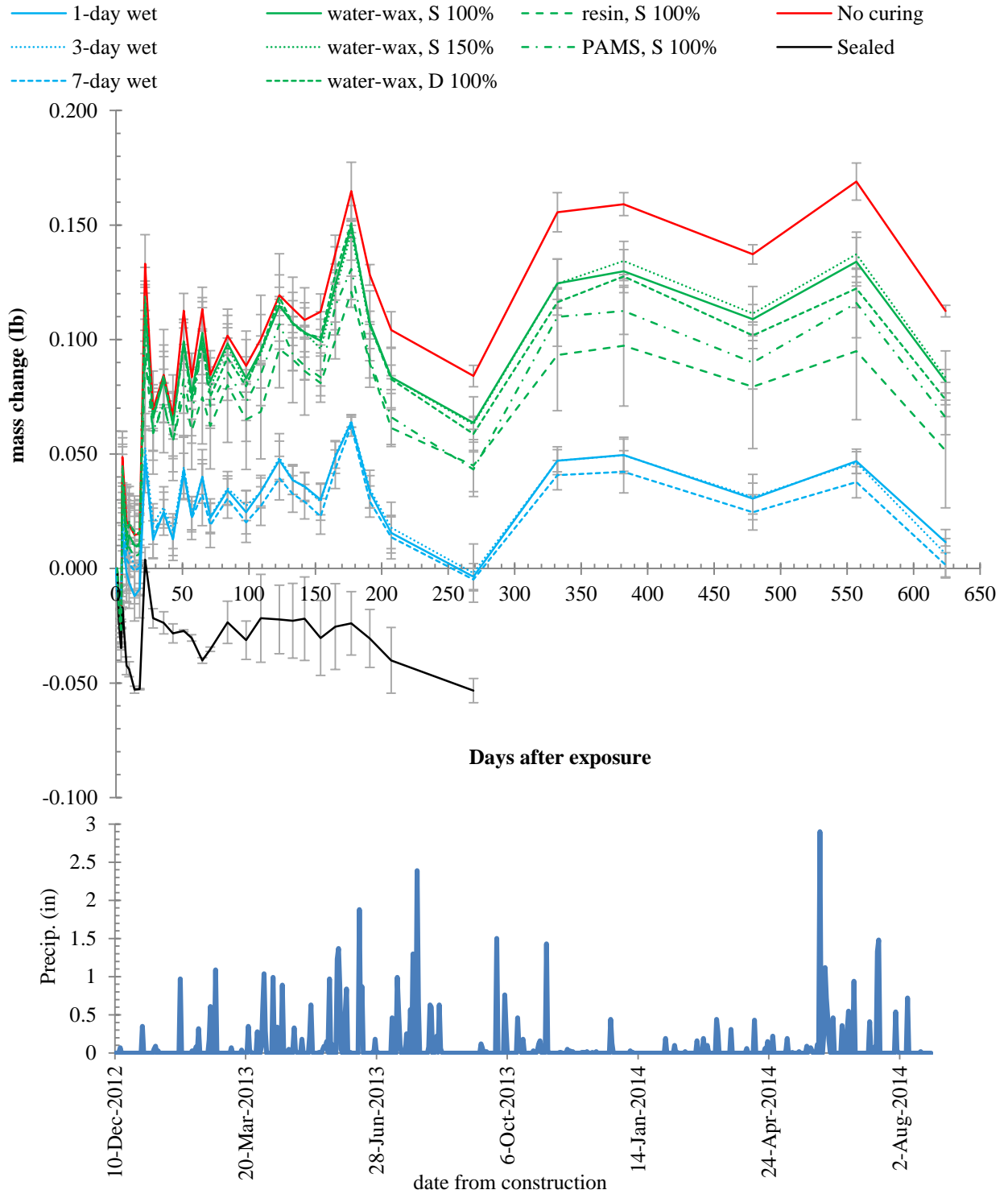








**Figure 12** shows the mass change of the beams and the rainfall events over days exposed to drying. The mass change values are the average from three samples. The positive values of mass change are due to increase in weight after rainfall.



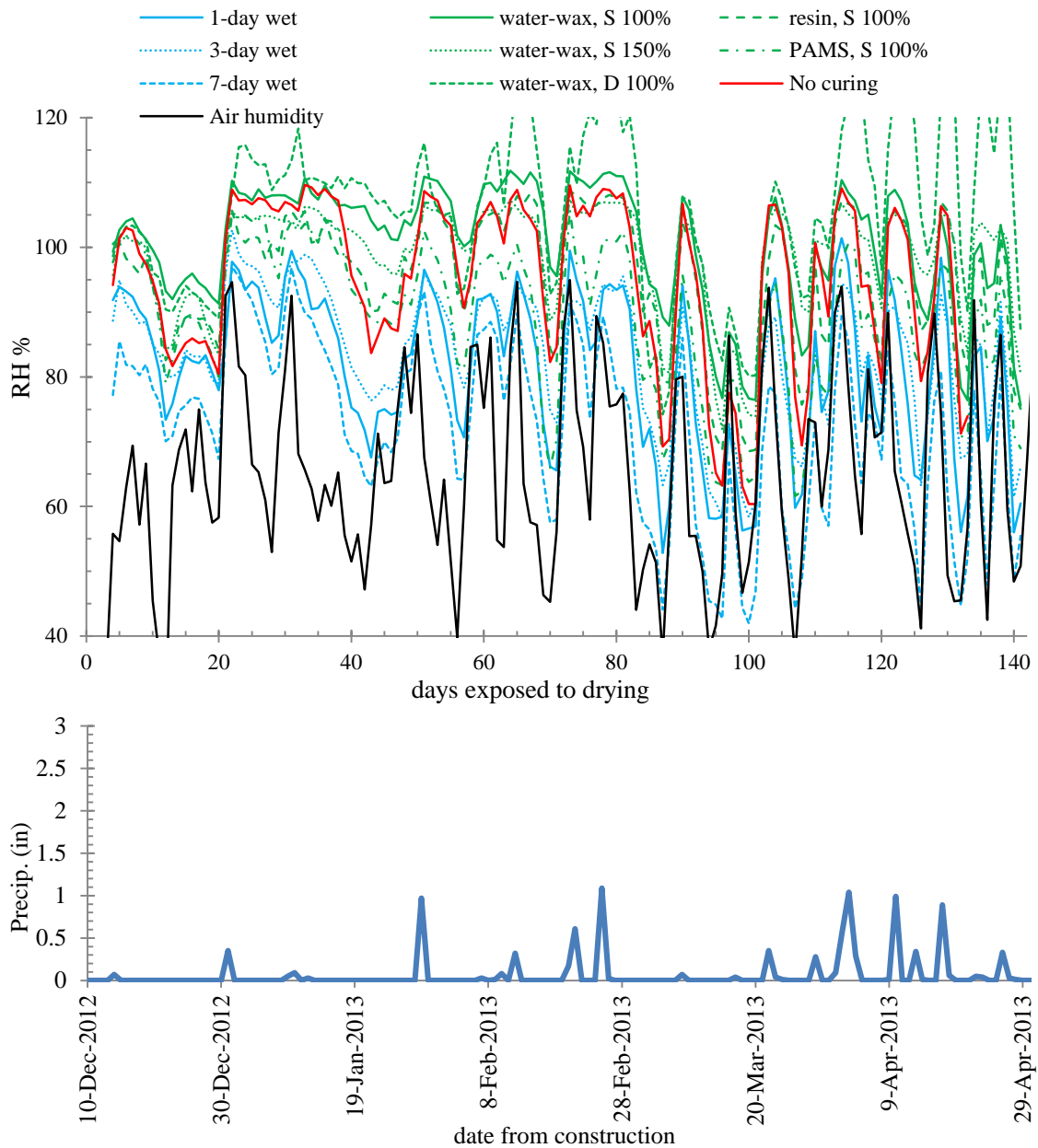
**Figure 12 - The mass change of the concrete specimens and rainfall events at the exposure site**

**Table 9** shows images of the surface of the curing compound samples after 100 and 190 days.

**Table 9 - The surface of cured samples with different curing compounds after 100 and 190 days**

After 100 days	After 190 days
Poly-alpha-methylstyrene based curing compound	
	
Resin based curing compound	
	
Water-wax based curing compound (100% double)	
	
Water-wax based curing compound (150%)	
	
Water-wax based curing compound (100%)	
	

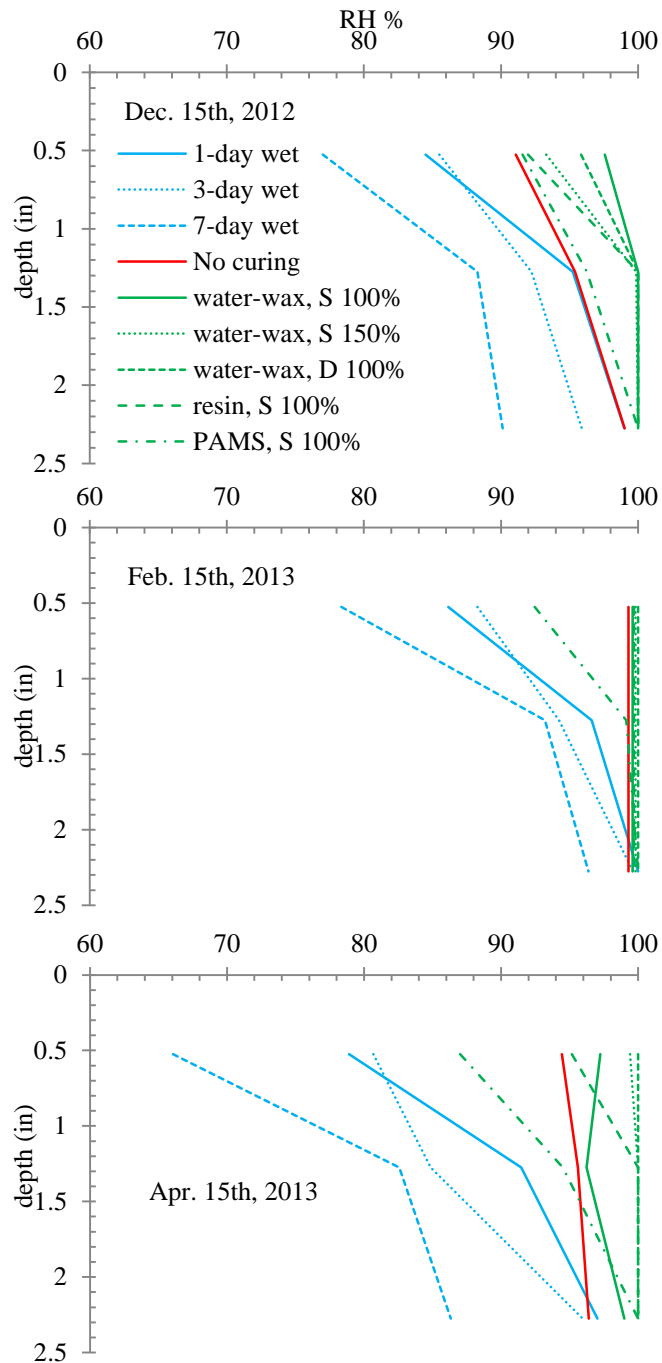
**Figure 13** shows the daily average RH at the top of the specimens over days exposed to drying in the field for different curing techniques. The bottom figure shows the rainfall amounts and the dates that they occurred.



**Figure 13 - The average RH at the depth 0.525” and the rainfall events**

**Figure 14** shows the RH profiles over the depth in the middle of three months December, February, and April.

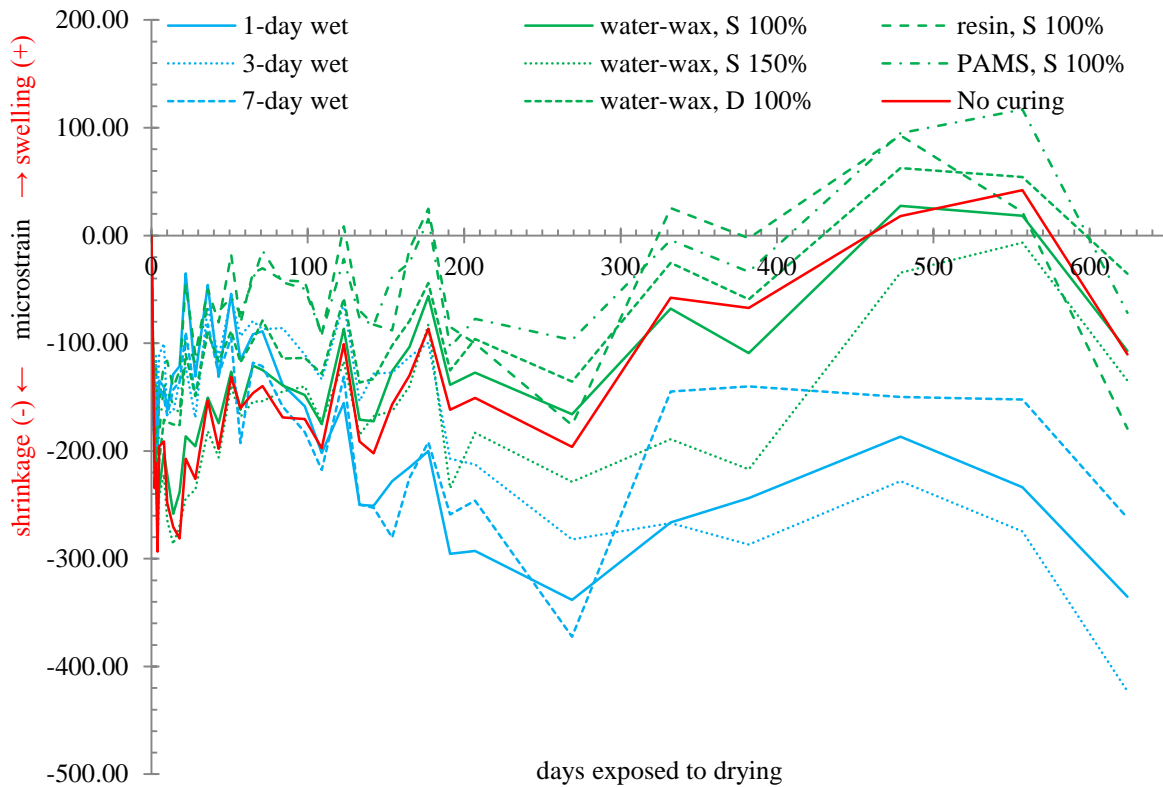




**Figure 14 - Average RH profiles for different curing methods**

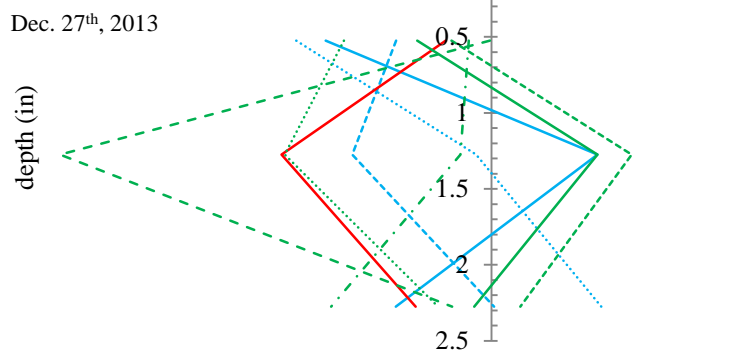
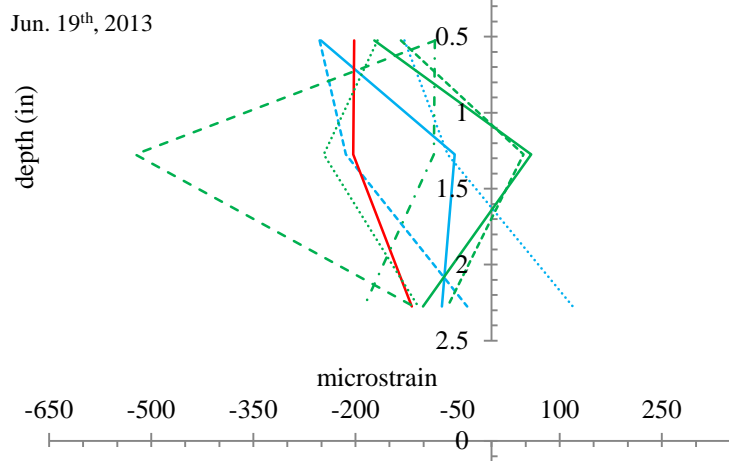
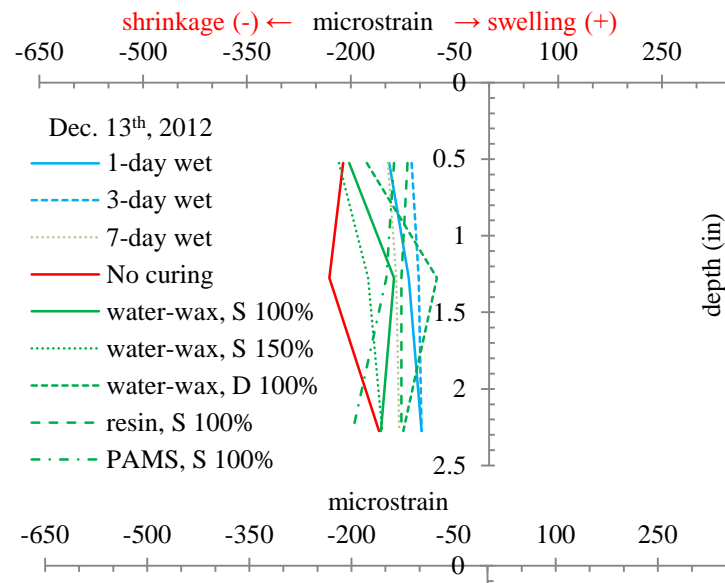
**Figure 15** shows the strain at 0.525" from the surface over time outside. It should be noted that negative values show the shrinkage while the positive values are the amount of swelling or expansion in the beams. The strain values are the average amounts from the three samples used for each method. Also, the graph

shows the strain from the moisture gradient, which is the total measured strain excluding the strain due to the differential temperature. A thermal expansion coefficient  $5.5 \times 10^{-6}$  in/in °F has been used to make this correction.



**Figure 15 - Strain at a depth of 0.525” of the concrete after being exposed**

**Figure 16** shows the strain profiles over the depth at every six months for the strain values modified with the thermal strain as mentioned above.



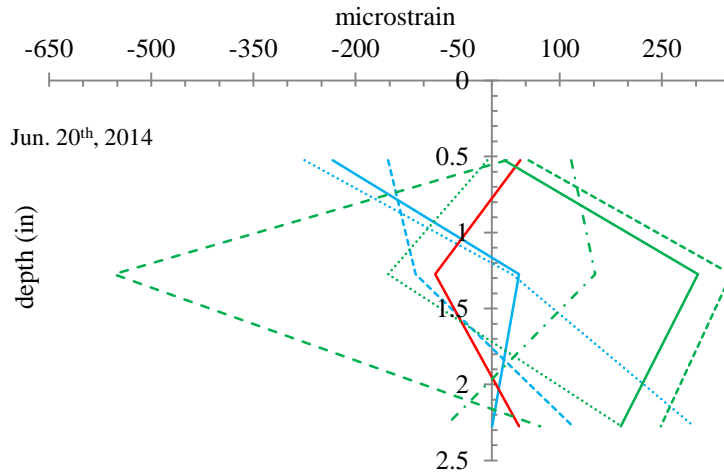


**Figure 16 - Average strain profiles for different curing methods**

### 3.5 DISCUSSION

#### 3.5.1 Weather Condition in the Field

The temperature change in the field is shown in **Fig. 10** for about five years in Oklahoma City. As can be seen the average temperature showed an increase over the summer time. The test was started in December 2012 when the weather was colder with considerable amounts of rainfall. **Figure 11** shows the RH for the same duration in this study; in general, the average RH has not significantly changed over the length of the test. Since the RH was observed to be around 65% during this field test another set of laboratory tests was done in a constant temperature and  $70 \pm 3\%$  RH inside a chamber room as shown in Chapter 2.

#### 3.5.2 Mass Change

**Figure 12** shows the weight change of specimens after exposure. There were some problems with the samples sealed with wax. The wax does not appear to be totally effective and the sample started to change in weight. After four weeks the sample was placed in a plastic bag. This was found to be a good solution to stabilize the weight loss of the sample. The mass change of the wet cured specimens

indicates that they all had similar mass change. Furthermore, the samples with curing compound also showed similar mass loss; however, there was a distinct difference between the results of these two samples. Specimens cured with curing compounds and the specimen that was not cured showed more mass change compared to wet cured and sealed specimens. The permeability of the wet cured specimens is expected to be lower than the no cured specimen and that of specimens cured with curing compounds. Due to a high RH in the field it is expected that the pores at the surface have only partially dried and so therefore show a lower amount of shrinkage. On the other hand, the specimen that was not cured has a higher permeability compared to the other specimens and consequently more weight gain after each rainfall, as shown in **Fig. 12**.

Specimens that were cured with curing compounds absorbed more water than the wet cured specimens. Specimens cured with water-wax based curing compound and different application rates have a very similar performance. Water-wax based curing compound with different amounts of coverage show statistically similar performance and absorbed more water than the other two curing compounds. This may have happened because it is a water-wax based coating and can be less durable under rain compared to resin and PAMS based materials. As shown in **Table 9**, it has been observed after 100 and 190 days that resin and PAMS based curing compounds still remained on the surface, while the water-wax based curing compound has been eroded partially or completely. Moreover, the reason that resin based curing compound look like an eroded surface is due to its high stickiness during application, which makes it more difficult to be applied consistently. However, it has remained on the surface throughout the period investigated.

### 3.5.3 Relative Humidity Change

**Figure 13** shows the RH at the top of specimens (depth 0.525"). The general trend between the beginning and the end of five-month exposure shows very little change in RH within the concrete. It should also be noted that the RH at the surface of the concrete follows the atmospheric RH but is a little higher. Because the concrete does not appear to be drying this suggests that the negative impacts of moisture gradients and their intensities should be minimized. This means that differential curling from drying shrinkage is not expected to be a major problem in a RH close to 65% as was observed during this testing period. High RH in the field together with precipitation can maintain the moisture in the samples. For this test this also seems to diminish the expected differences between the effectiveness of different curing methods. However, even with the higher RH the wet cured samples have the highest shrinkage. This is in agreement with the findings from phase one of this study and chapter 2.

**Figure 14** shows the RH profiles of the specimens at the middle of December 2012, February 2013, and April 2013; the red line shows the profile for specimens without curing. As discussed above, wet cured specimens have less internal humidity compared to specimens with curing compounds. The lower permeability of the wet cured specimens should be the main reason for this difference. Curing compound specimens have a very high internal humidity (above 90%) and less moisture gradients compared to wet cured specimens due to more moisture gain after each rainfall.

### 3.5.4 Strain Change

**Figure 15** shows strain changes at the top of specimens where the positive values show swelling and negative values show shrinkage. The thermal strain has been removed from the total strain in this figure. The strain fluctuates at different periods of time because of the rainfall events as shown below the graph. The specimens in general tend to swell due to an increase in moisture after each rain.

**Figure 16** shows the strain profiles every six months during the test; the strain gradients of specimens cured with curing compounds are not as large as the slopes of wet cured specimens, which might be caused by a finer pore structure at the surface of the wet cured specimens that makes them more impermeable to external water. This leads to a less moisture gradient in curing compound samples, as seen in **Fig. 14**.

## 3.6 CONCLUSION

The impact of ambient weather condition has been observed on samples cured with different methods; the following observations were made:

- The average temperature in Oklahoma City has consistent fluctuations each year with the highest peak around August of each year, while the average RH has not changed over the five years and remained on average to be about 65%.
- The wet cured samples showed less mass change than the samples with curing compound and no curing.
- Surface of samples cured with PAMS based curing compound and resin based curing compound have not significantly changed after long term

exposure, while surface of samples cured with water-wax based curing compound has been considerably eroded after five months of exposure.

- Drying shrinkage would not be expected as a major reason for strain changes in RH conditions that are on average 65% as is the case in Oklahoma. In this environment a gradual ambient temperature and moisture raise can make the samples swell where the high RH minimizes the intensity of the drying condition.
- Different curing compounds perform very similarly in the above mentioned condition and strain changes are statistically similar, which were caused by continuous fluctuations in temperature and RH during the test.

This data continues to confirm that when the field RH of concrete is near 65% then the curling strains caused by drying are minimal because the concrete does not significantly dry. This means the type of curing that is used on concrete pavements in Oklahoma will have very little impact on their curling deformations. However these curing methods may have an impact on a number of other important concrete properties such as the strength, permeability, and abrasion resistance.



# CHAPTER 4 – INSTRUMENTATION OF I-44 AND LEWIS

## 4.1 INTRODUCTION

In order to learn more about the impact of different curing methods on the curling of concrete pavements in the field 62 different sensors were installed on a continuous reinforced concrete pavement used on Highway I-44 & Lewis in Tulsa, Oklahoma in August of 2013. The pavement was 12” in depth and 14’ in width. Another outside lane is planned to be paved later. This outside lane is not reinforced.

## 4.2 INSTRUMENTATION

The goal of the research was to compare four different curing methods and the impact they have on the curling of concrete pavements. **Fig. 17** shows the truck mixer and the paver used on the project.



**Figure 17 - Casting the concrete pavement**

The following curing methods were investigated as shown in **Fig. 18**: wet cure with wet burlap for 5 days, water-wax and PAMS curing compound, and misting

provided to the surface of the pavement every hour for 24 hours. Nine strain gages and seven RH sensors are used to measure the strain and RH profiles of a typical slab.

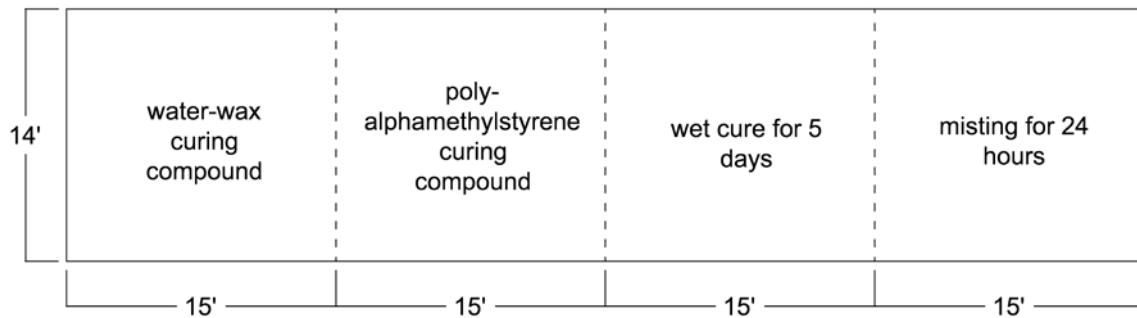


**Figure 18 - Curing materials and methods used on the pavement**

**Figure 19** shows the arrangement of the strain gages and rebar. Each gage can measure strain and temperature simultaneously. These gages were chosen because they were robust and have been used for long term monitoring of concrete structures. These strain gages were tied to a vertical stand with feet at the bottom to help hold the bars in place. This stand was then tied to the traverse reinforcing bars. Care was taken in the field to ensure that each gage was at the reported height from the concrete base shown in **Fig. 19**. However, it was not possible to measure these sensors after the fresh concrete was placed and consolidated and so it may be possible that small changes occurred that were not captured. It should also be noted that the actual pavement constructed was 13” instead of 12” at the point of construction. This slightly changes the strains measured in the pavement but should be able to be overcome in the analysis of the data.

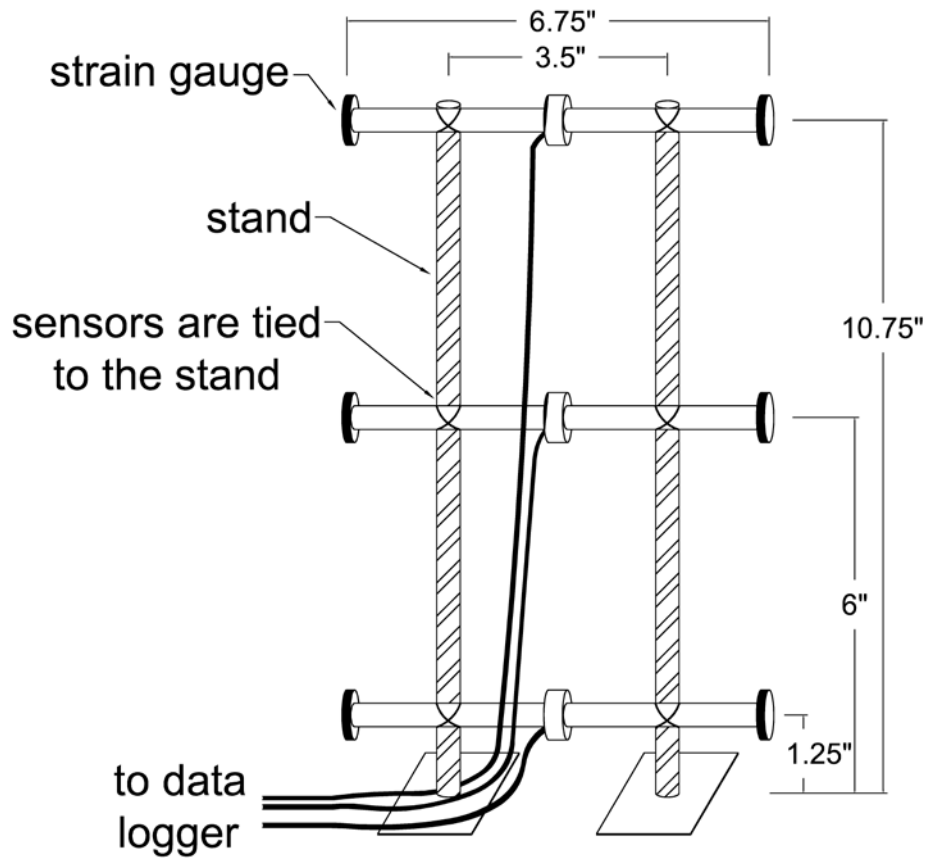


**Figure 19 - A strain gage tied to the steel bars**

The RH gages were placed at two different spots, which are the centerline between each two sets of strain gages. RH is measured at different depths: 1", 3.5", 6", and 11" as shown in **Fig. 20**.

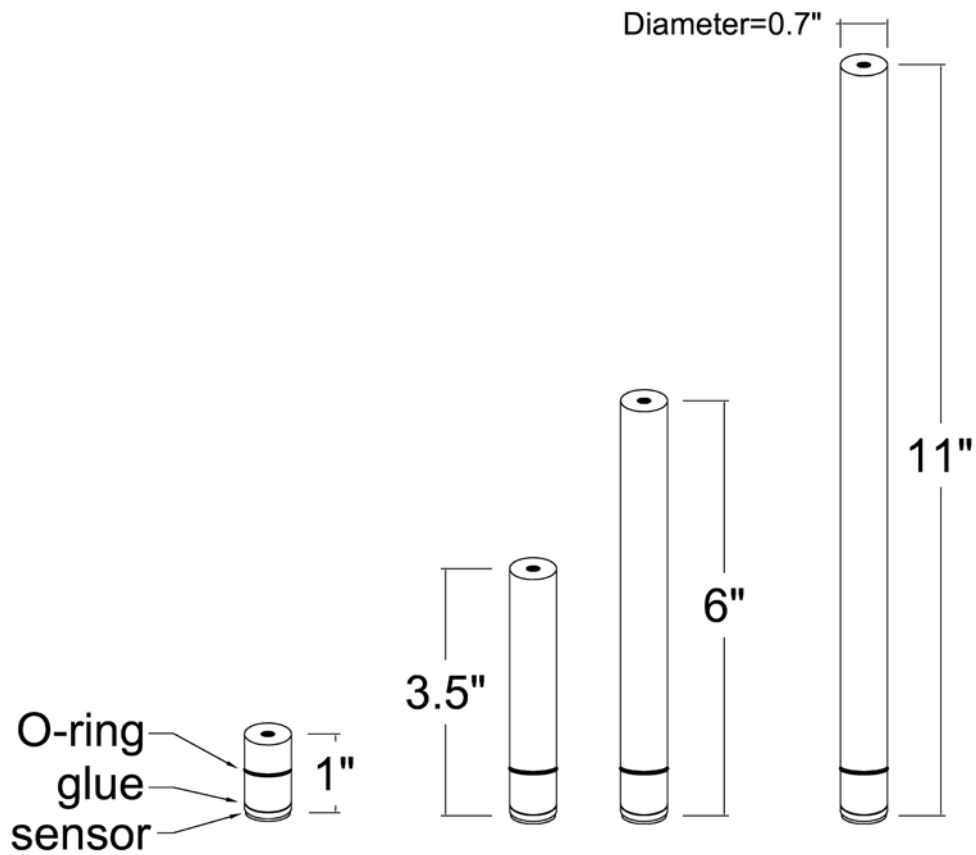


**Figure 20 - RH sensors glued to rods**

The sensors at 11" were measured only for wet curing and the water-wax based curing compound. The mentioned depths were drilled in the pavement five days after paving. Sensors were glued to rods that were embedded into the drilled holes. These rods had an O-ring at the end to seal between the concrete and the rod to ensure that the readings were only coming from the concrete near the sensor. Grease and caulk was also used to help seal the rod. A typical installation is shown in **Fig. 20**.

Strain gages were embedded in the pavement at three different spots. Nominally the gages were attempted to be placed at the center, edge, and the quarter point of the pavement. Unfortunately because of the rebar layout and

pavement vibrators these locations had to be varied slightly. As shown in **Fig. 21** for a typical slab, the gages were oriented in the transverse direction of the pavement in order to measure curling and shrinkage of the pavement. A gage was used at the top and bottom of the pavement so that it could show any differential strain between these two locations. This strain differential will be tied to the amount of curvature or bending that occurs in the pavement. The strain gage at the center of the pavement will help examine the strain profile and the amount of uniform shrinkage that occurs in the pavement. By combining these measurements with the temperature measurements and humidity, it should be possible to compare the overall strain profiles in the pavement and determine whether these can be attributed to differentials in shrinkage, temperature, or humidity.

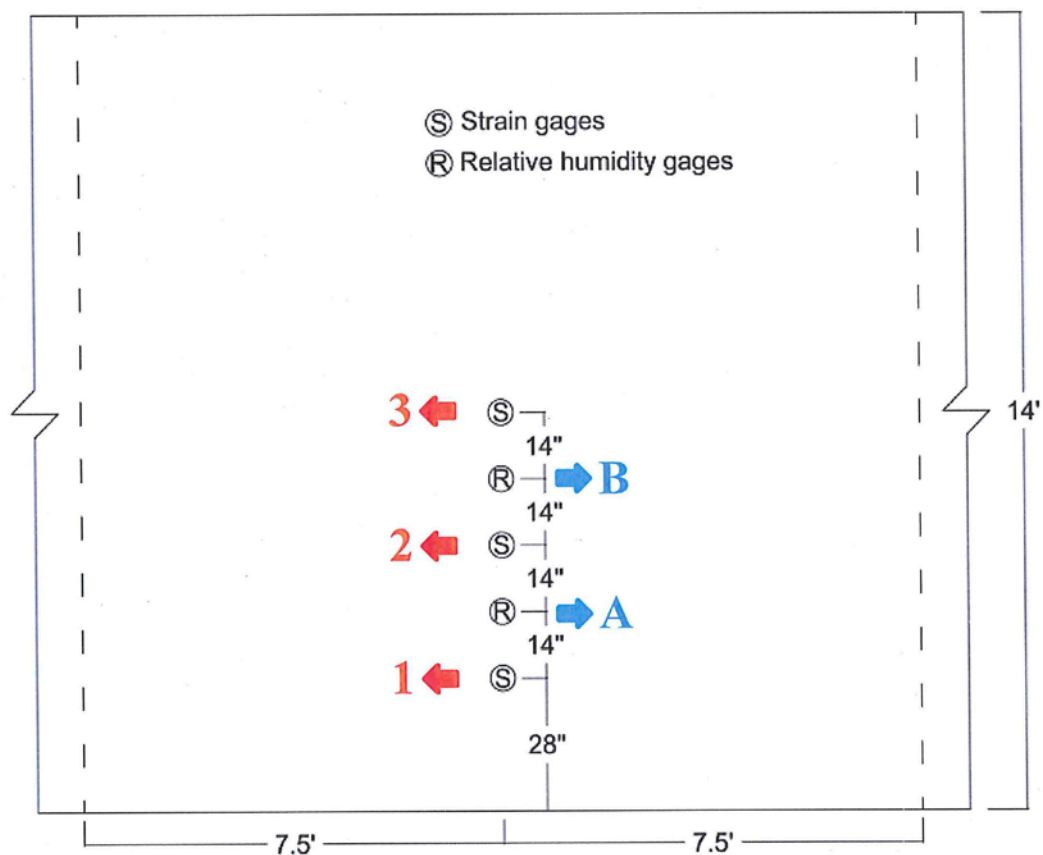


**Figure 21 - Top view of a typical slab to show the coordination of all the gages**

The gauges as placed in the pavement are shown in in **Fig. 22**.



**Figure 22 - The strain gage locations for each curing method**

#### **4.3 APPLICATION OF THE CURING METHODS**

Both of the curing compounds were manually applied to the surface of the pavement. The water-wax based curing compound was sprayed manually by the contractor and the PAMS was sprayed by the researchers. Examples of their sprayed surfaces is shown in **Fig. 23** and **24**. **Figure 25** shows the wet burlaps under the white plastic sheet to cure this section of the pavement for five days. After five days and before drilling, the curing was terminated and the burlaps were still moist. The last section of this field experiment was cured by using misting. This was done manually every hour for the first 24 hours after placement of the concrete.



**Figure 23 - The water-wax based curing compound applied by the contractor approximately 30 minutes after paving**



**Figure 24 - PAMS curing compound applied by the research team**



**Figure 25 - Wet curing for five days under white plastic sheets**

While constructing the shoulder concrete on the project a heavy rainstorm destroyed the surface finish of the concrete. The contractor had to remove and replace the shoulder. In doing this the wiring for three gages were destroyed.

#### **4.4 RESULTS AND DISCUSSION**

Using a running average for every 6 hours from paving the temperature profiles have been calculated from the measured data. The running average has been used to reduce the fluctuations of the data measured with the strain gages over the time. Temperature profiles of the slab are shown in **Fig. 26, 27, and 28** respectively for locations 1, 2, and 3 in **Fig. 21**. These locations are at 28", 56", and 84" from the edge of the slab, respectively. The profiles are for ages 0.1, 30, and 100 days after paving.



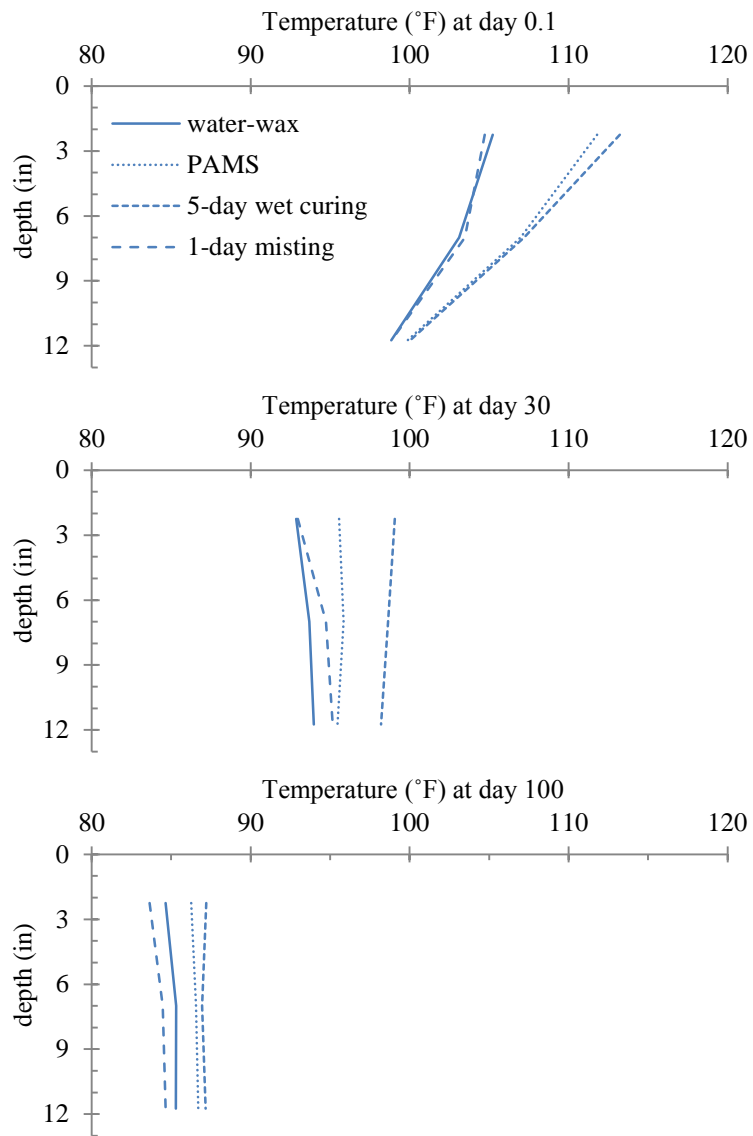


**Figure 26 - Temperature profiles for location 1 at 0.1, 30, and 100 days after paving**

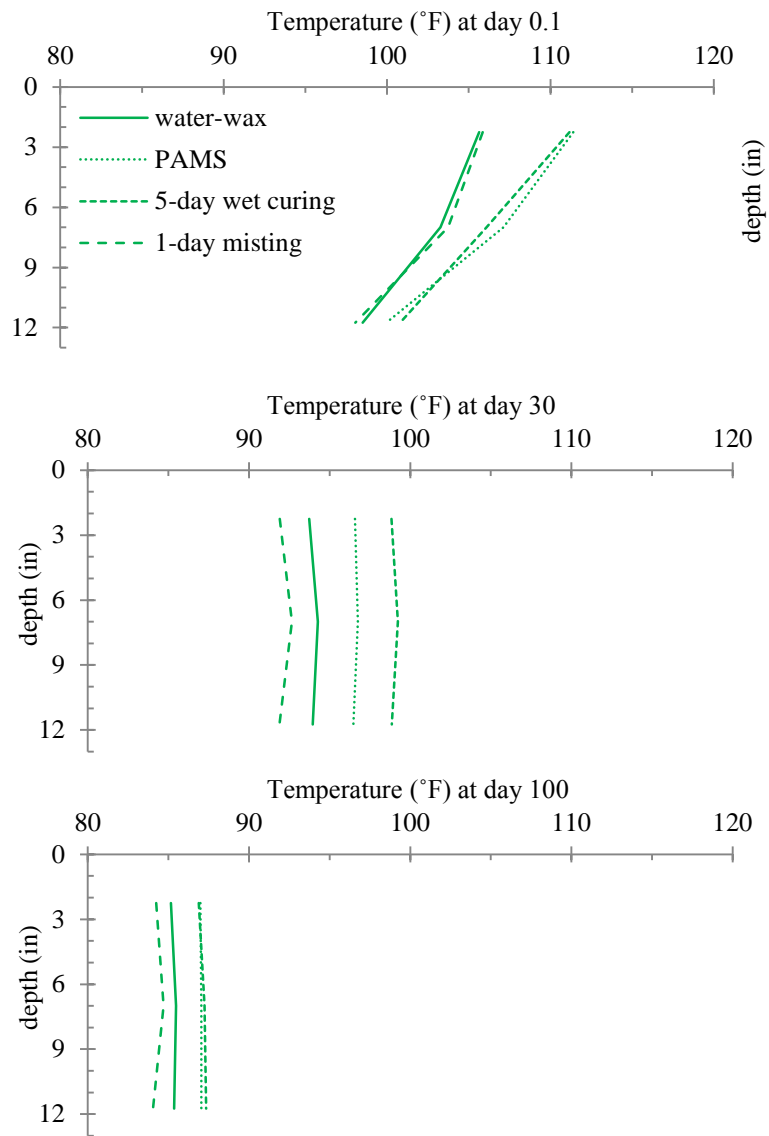


**Figure 27 - Temperature profiles for location 2 at 0.1, 30, and 100 days after paving**

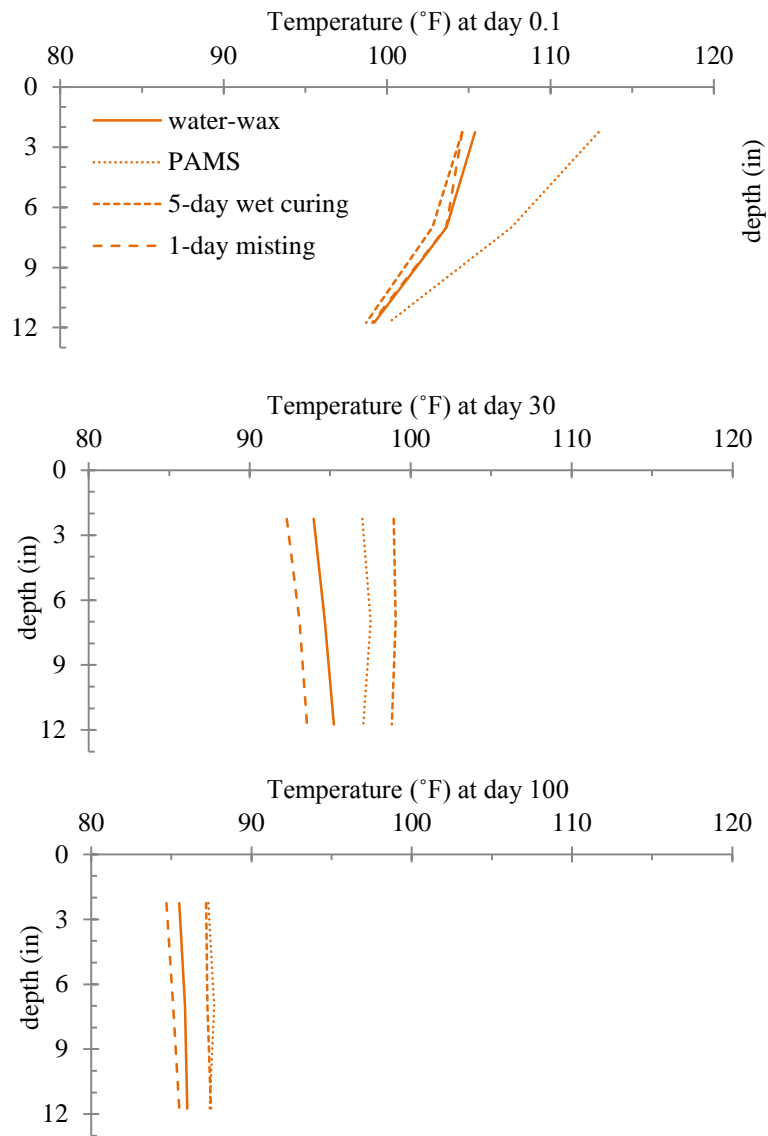


**Figure 28 - Temperature profiles for location 3 at 0.1, 30, and 100 days after paving**

The temperature gradient is the most at early ages; for examples, about 0.1 day after paving the temperature gradient within the slabs cured either with the PAMS curing compound or the 5-day wet curing is noticeable. However, the gradient becomes negligible over the time for all curing techniques. This low temperature gradient leads to less warping deflections.

Moreover, the temperature is always higher in 5-day wet curing and PAMS and lower in water-wax curing compound and 1-day misting. A higher temperature

may lead to expansion within the slab, which will be shown later. After 100 days this difference has become less as well.

Finally, comparing the three graphs, it should be pointed out that the temperature and its gradients are the same in all sections 28", 56", and 84" from the edge of the slab at all edges, which leads to the same thermal stresses. Also, the slab experiences a temperature gradient due to the daily temperature change and therefore a small strain gradient. But since a running average has been used, this daily temperature gradient has not been shown here.

**Figures 29, 30, and 31** show the strain profiles of the slabs cured with different techniques for the marked locations 1, 2, and 3 of **Fig. 21**. These locations are at 28", 56", and 84" from the edge of the slab, respectively. A running average for every 6 hours has been used. The profiles show the strain gradients within the slab for 0.1, 30, and 100 days after paving. The positive values show the swelling and negative values are for shrinkage.

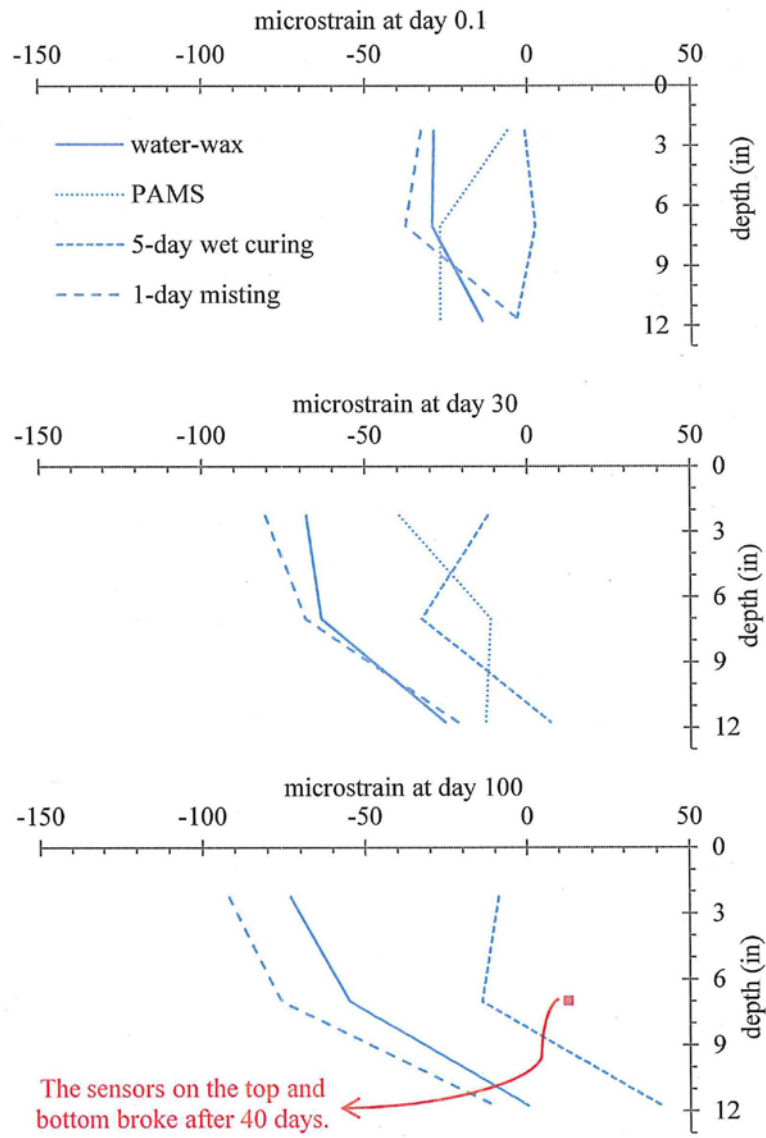


**Figure 29 - Strain profiles for location 1 at 0.1, 30, and 100 days after paving**

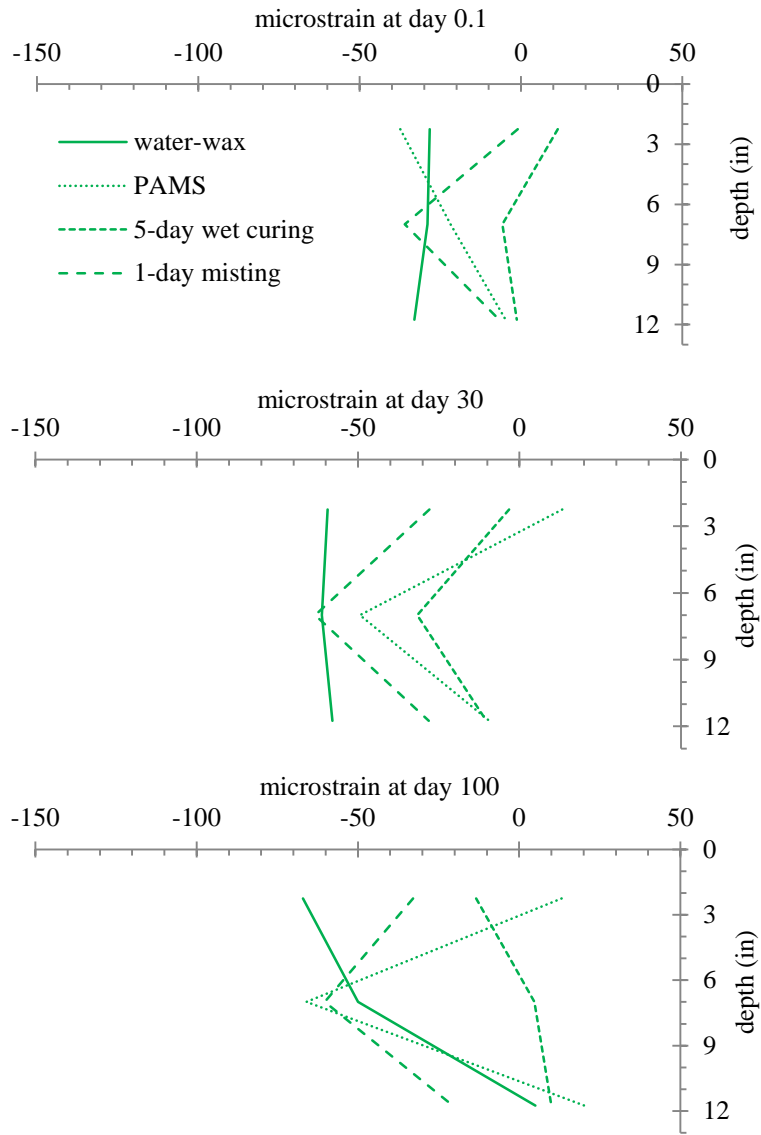


**Figure 30 - Strain profiles for location 2 at 0.1, 30, and 100 days after paving**

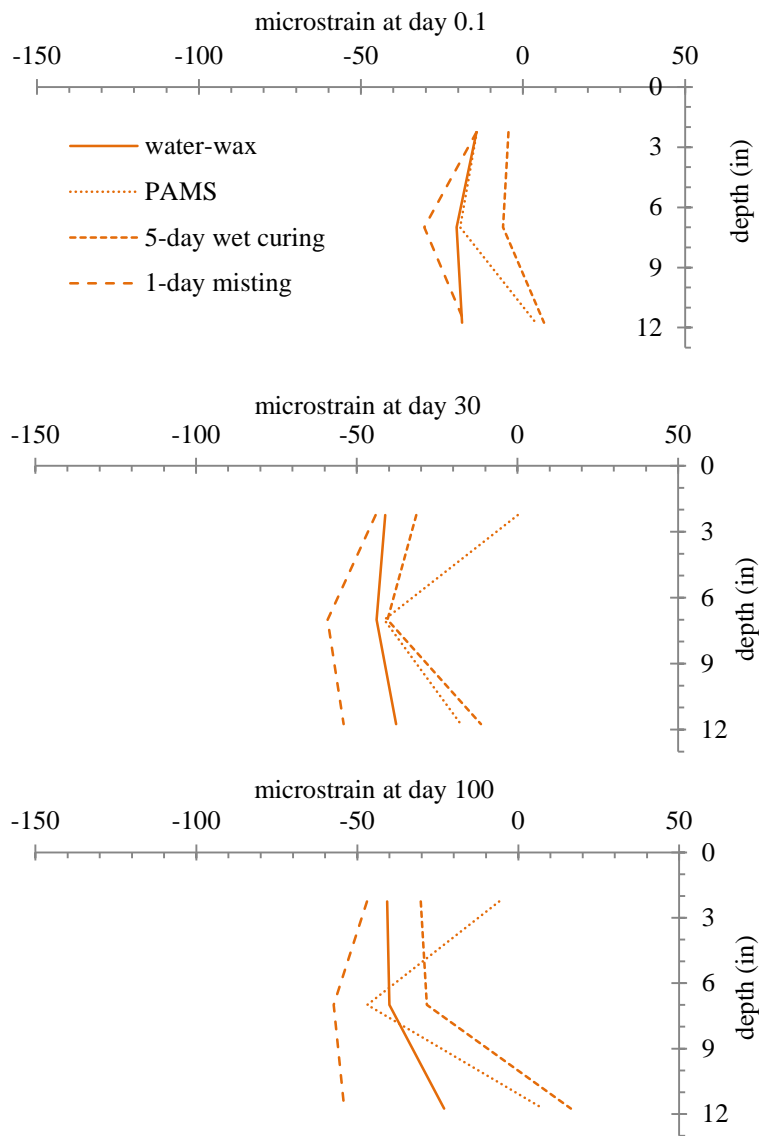
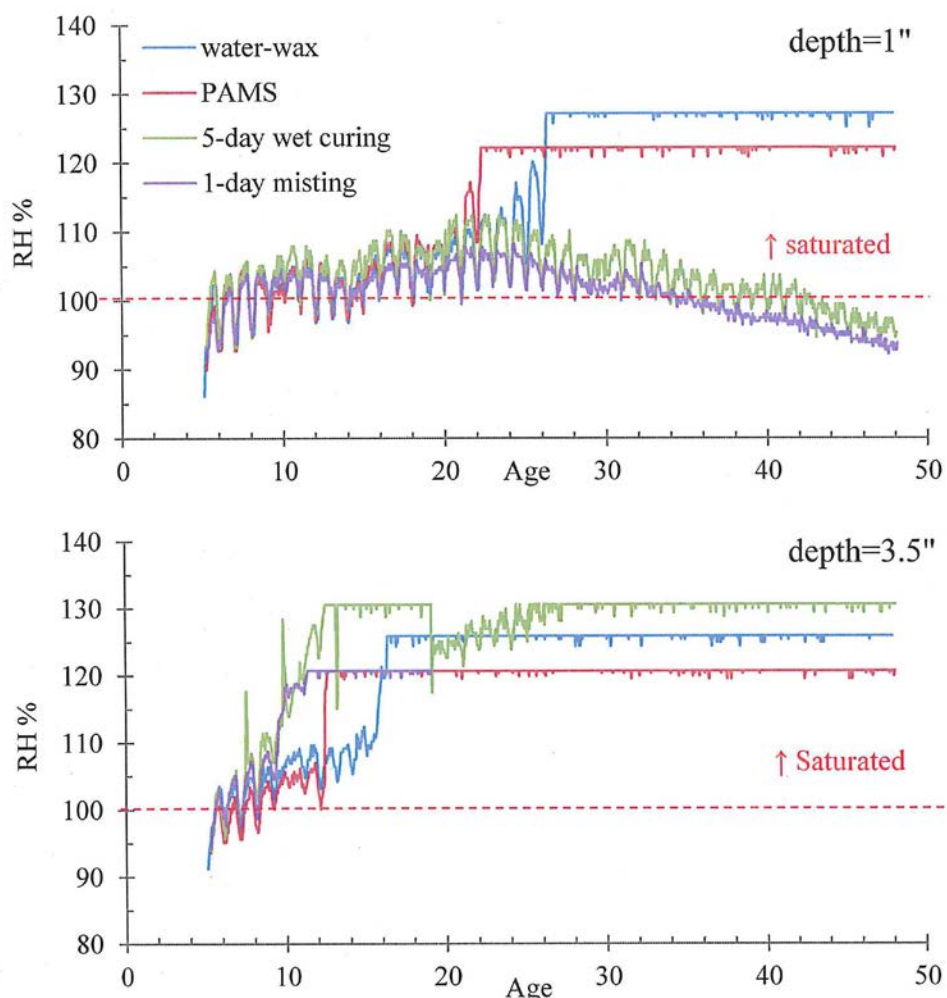


**Figure 31 - Strain profiles for location 3 at 0.1, 30, and 100 days after paving**

Based on **Figs. 29, 30, and 31** it appears that there is significantly more curling that is occurring at the edge of the pavement than is happening in the middle. This could be caused by moisture or temperature gradients. However, based on the measured temperatures in the pavements this gradient is likely caused by moisture. This curling does not appear to be caused by the type of curing. Instead it appears to be caused by a large moisture gradient in the pavement. During construction the water table was observed to be very near the surface in this pavement. This means that the bottom of the pavement is likely wet while the top dries. This creates a large

gradient in the pavement and leads to the increased curling that is observed. This curling may become a problem over time and should be watched closely.

As mentioned earlier in the instrumentation section, several RH sensors at different depths of the slab were used at the marked locations A and B in **Fig. 21**. These sensors broke due to the very high RH over the depth of slab after about 30 days. This might be due to either a very high water level underneath the road or the penetration of the water through the drilled holes. Therefore, the RH values higher than 100% or the data after 30 days are not valid. As an example, the changes in RH at location B are shown in **Fig. 32** for different depths.





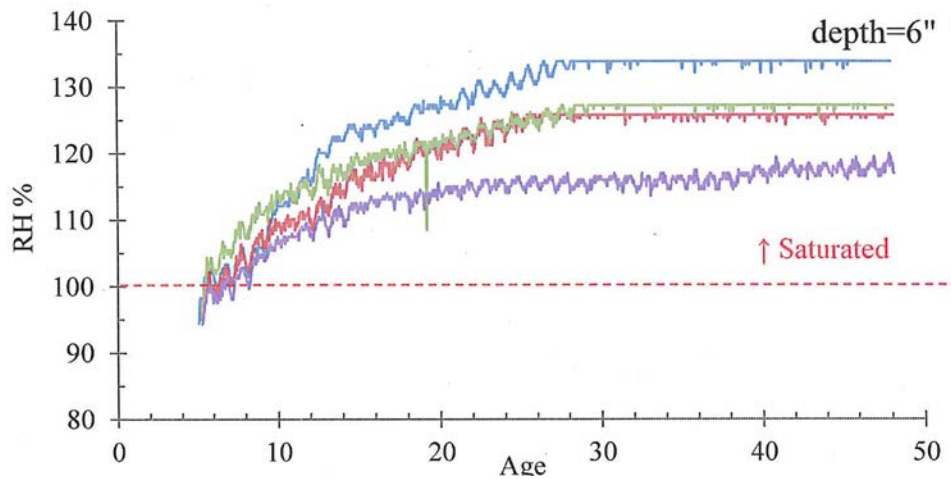


**Figure 32 – RH over the time for location B at different depths**

The RH at depth 1" as shown in Fig. 32 starts to decrease around 40 days from paving for 1-day misting and 5-day wet curing. However, the sensors show saturated conditions for the other depths and curing methods. It seems that these other sensors have been destroyed. Because of this it is difficult to draw conclusions from this data. The observation that the slab has very high moisture content is confirmed because of the malfunctioning of so many gages due to moisture.

#### **4.5 CONCLUSION**

In this chapter the instrumentation of a concrete pavement has been reviewed. The pavement was instrumented to measure strain, temperature, and relative humidity at the pavement center, edge, and then at an intermediate point. The data shows that the temperature gradient is almost constant in the pavement. However, the strain gradient is not. The strain at the edge of the pavement is much higher than the middle. This is likely caused by a significant moisture gradient in the pavement that is caused by a very high water table. The relative humidity sensors were destroyed in this work because they were too wet. The pavement will continue

to be monitored in the next part of the project to determine the long term performance.

## **CHAPTER 5 - SENSITIVITY ANALYSIS OF DARWIN-ME TO BASE FRICTION**

### **5.1 INTRODUCTION**

Base-slab friction is the design input which affects the performance of Continuous Reinforced Concrete Pavement (CRCP) and Jointed Plain Concrete Pavement (JPCP). To determine the importance of the friction on the long term performance of Oklahoma pavements we conducted a sensitivity analysis by using the DARWin-ME software.

For CRCP DARWin-ME allows the user to input a base friction coefficient and for JPCP the user determines the amount of time necessary before the pavement loses friction. The sensitivity analysis was completed by selecting different base slab parameters for both CRCP and JPCP sections with different thicknesses, joint spacing and Average Annual Daily Truck Traffic (AADTT). The pavement properties were chosen as they were representative of Oklahoma pavements and the AADTT was chosen so that they were at the design limit for that section.

An overview of the sections used is given in **Table 10, 11, and 12**. The AADTT used caused the designed pavements to be at the default failure criteria based on previous ODOT research. The variables used in table 1.3 represent a typical ODOT CRCP and JPCP section. The impact of the resilient modulus was also investigated by using values of 4,000, 8,000, and 12,000 psi, to study the effect of subgrade stiffness on pavement performance.

For CRCP the default value for the base friction coefficient is 7.5. Six different base-slab friction coefficients were investigated to better understand their impact on the performance of the pavement. For JPCP it is assumed that there is a full friction at the beginning but it is lost over time. DARWin-ME uses 240 months as the default value for friction loss. Six different values of friction loss at 75, 150, 229, 240, and 300 months were also investigated.

**Table 10 - CRCP Sections**

Section	AADTT	Thickness (in)
1C	25000	12.5
2C	23000	12
3C	14000	11
4C	9000	10

**Table 11 - JPCP Sections**

Section	AADTT	Joint Spacing (ft)	Thickness (in)
1J	8500	18	12.5
2J	5000	18	12
3J	2500	18	11
4J	1500	18	10
5J	25000	15	12.5
6J	21000	15	12
7J	14500	15	11
8J	9500	15	10
9J	25000	12	12.5

**Table 12 - Baseline Design Values**

design life	20 years
Cement	600 lbs of type I
concrete compressive strength	5000 psi
CTE	$5.5 \times 10^{-6}/^{\circ}\text{F}$
Curing	curing compound
Shoulder	Tied
JCP dowel diameter	1.5"
CRCP reinf. Ratio	0.70%
Location	Stillwater
pavement opening	Fall
base layers	4" asphalt 8" chemically stabilized base
Subgrade	8000 psi resilient modulus

## **5.2 DISCUSSION**

### **5.2.1 CRCP**

**Figures 18 and 19** show the effect of friction coefficient on terminal IRI and punchouts. All sections show that as friction increases terminal IRI and punchouts decrease. Note that as the friction coefficient increases over eight, there was no impact on the pavement performance except the 10" thick section which showed a minor improvement. It should also be noted that both the IRI and the punchouts per mile were sensitive to the friction coefficient used.

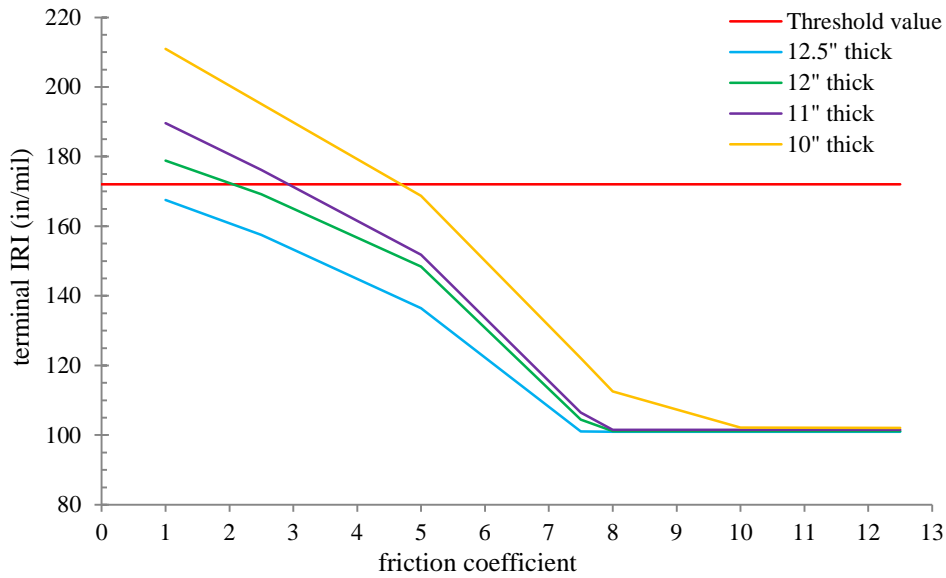


**Figure 33 - Terminal IRI vs. friction coefficient for CRCP with subgrade resilient modulus**

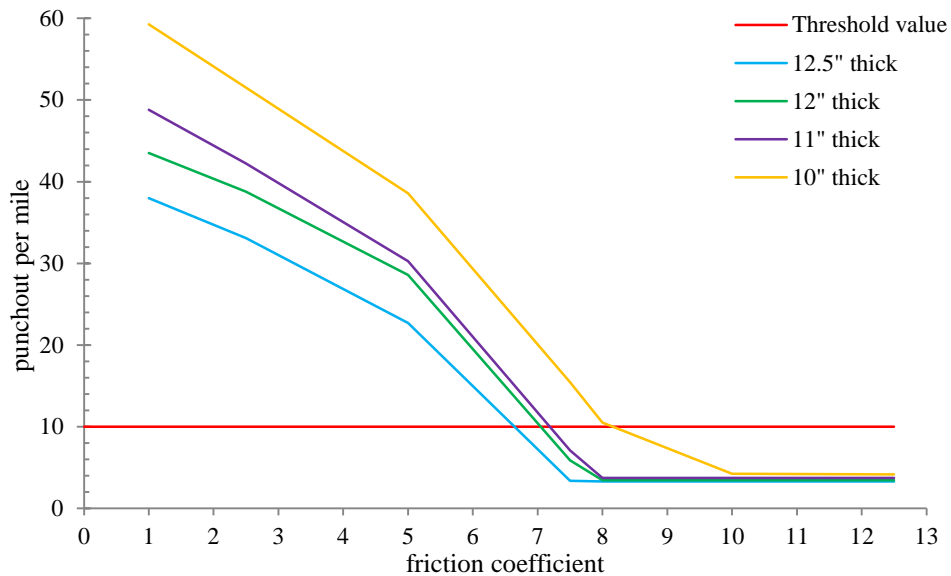


**Figure 34 - CRCP punchout vs. friction coefficient with subgrade resilient modulus of 8,000 psi**

All CRCP sections were also investigated with subgrade resilient modulus of 4,000, and 12,000 psi. **Figures 20** and **21** show the effect of friction coefficient on terminal IRI and punchouts of CRCP sections with softer and stiffer base.

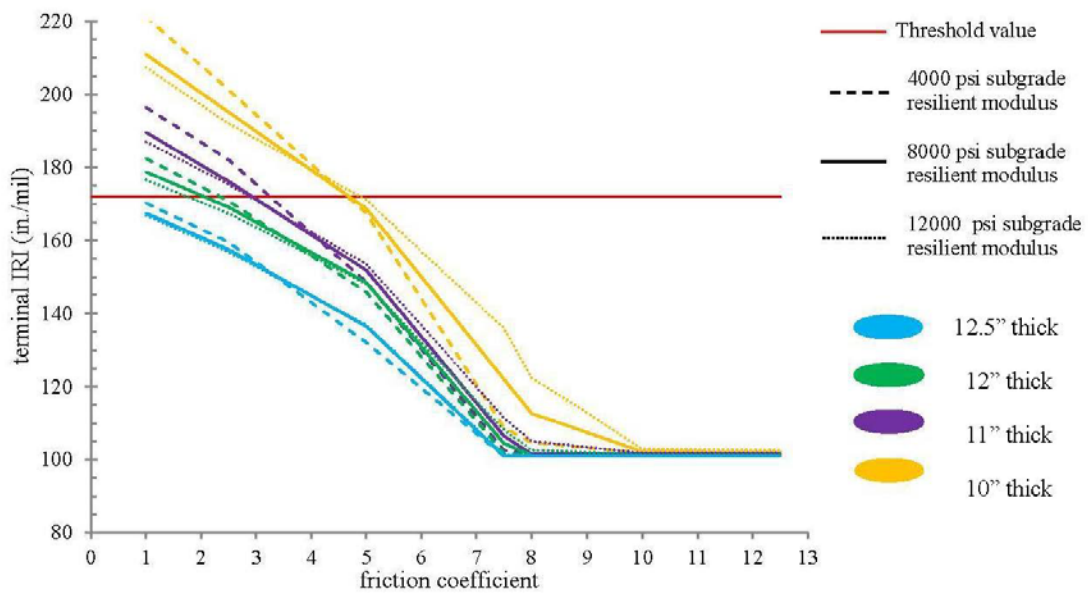


**Figure 35 - Terminal IRI vs. friction coefficient for CRCP with different subgrade stiffness**

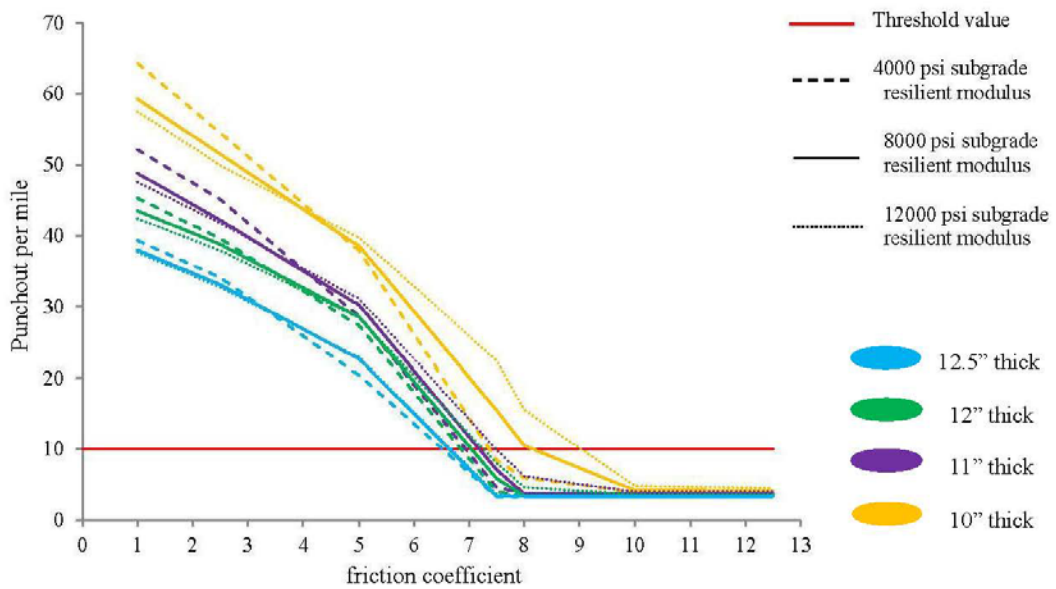


**Figure 36 - CRCP Punchout vs. friction coefficient with different subgrade stiffness**

From the changes in resilient modulus it shows that there is a little impact on the overall trend of the effect of the friction coefficient. It is interesting to note that for friction coefficients from 4 to 7 that the pavements with a resilient modulus of 4,000 psi had a better performance than the modulus that was 12,000 psi. This relationship changes once the modulus is below 4.

### 5.2.2 JPCP

Nine different JPCP sections with different thicknesses, joint spacing, and AADTT were investigated. The characteristics of each model are given in table 1.2. The effect of base friction loss on Terminal IRI and Transverse Cracking is shown in Fig. 22 and 23. Note that the base friction does not have any effect on Mean Joint Faulting. All graphs show that as the friction becomes effective for longer periods, the terminal IRI and slab cracking decrease.

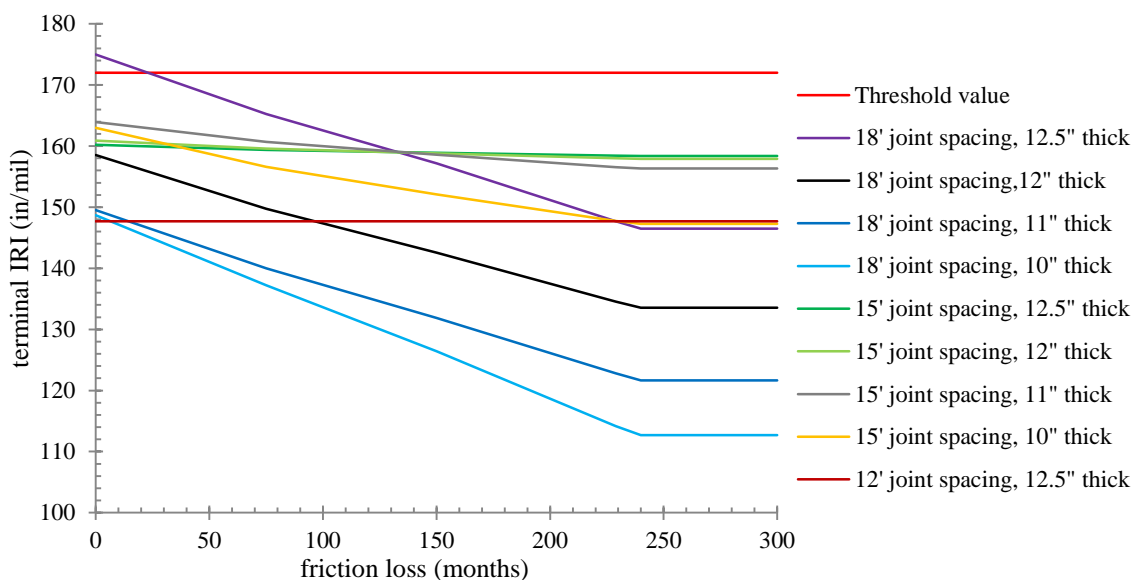


**Figure 37 - Terminal IRI vs. friction loss for JPCP with subgrade resilient modulus of 8000 psi**

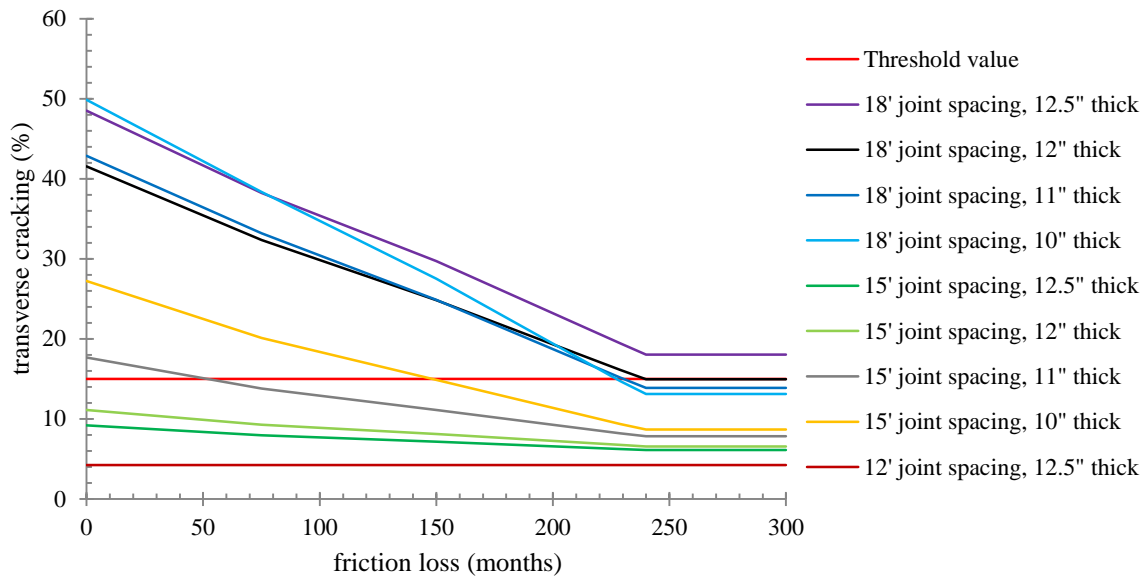


**Figure 38 - Transverse cracking vs. friction loss for JPCP with subgrade resilient modulus of 8000 psi**

The sensitivity analysis shows that after 240 months, which is the default value of DARWin-ME for friction loss, increasing the friction time does not result in any changes in the pavement performance for any of the criteria investigated. For IRI performance it appears that the slabs with a joint spacing of 18' are impacted by friction loss prior to 240 months; however, the slabs with a joint spacing of 15' and 12' are not. For transverse cracking the longer joint spacing also performed worse than the sections with a 15' and 12' joint spacing. For transverse cracking all of the pavements showed accelerated deterioration with early loss of base friction except for the pavements that had a 12' joint spacing, where very little increase in slab cracking was observed.

Next the impact of resilient modulus was investigated. This is shown in **Figs. 24 and 25**. This was done by investigating subgrades with 4,000, 8,000, and 12,000 psi resilient modulus.



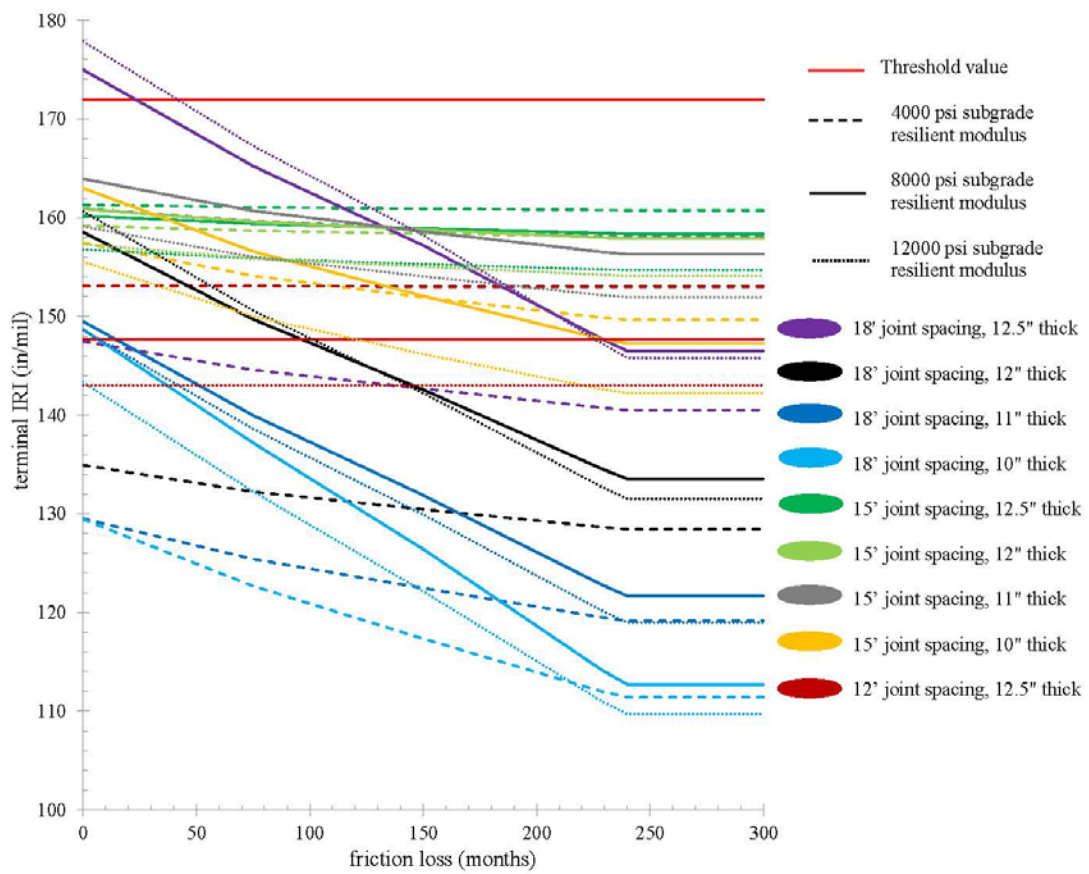


**Figure 39 - Terminal IRI vs. friction loss for JPCP with different subgrade stiffness**

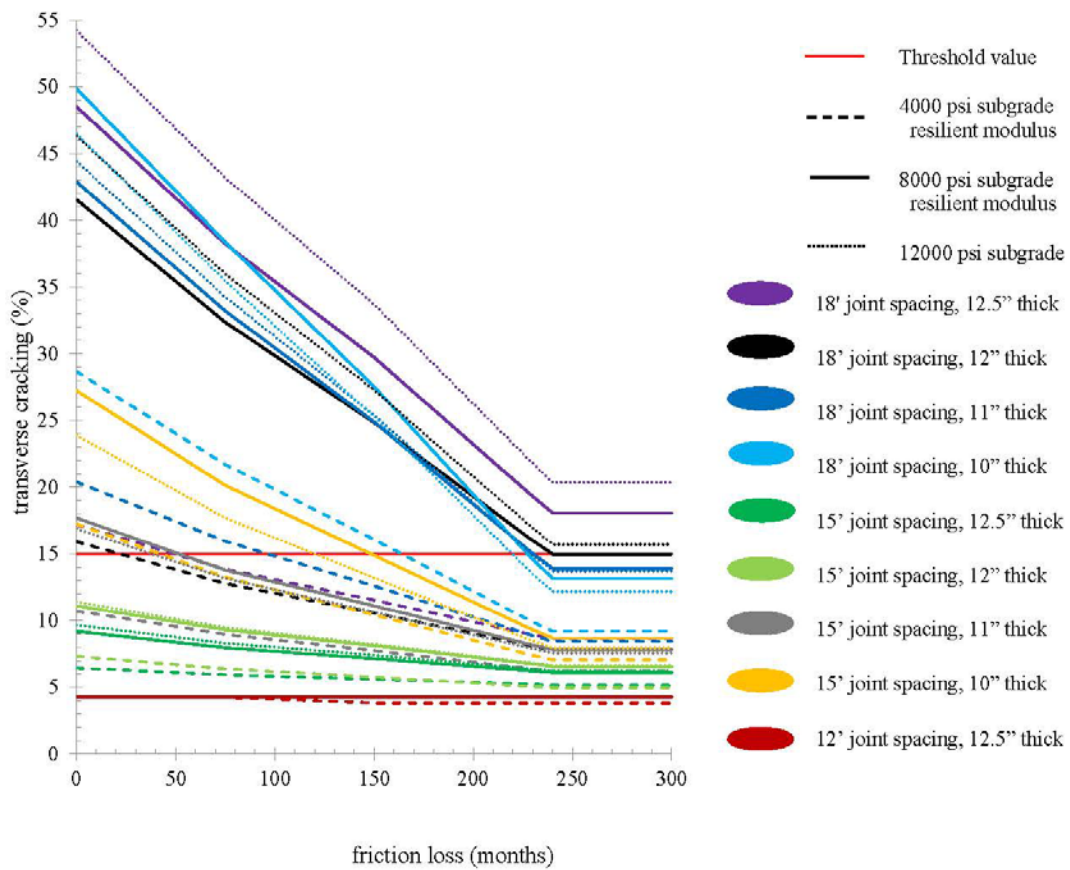


**Figure 40 - Transverse cracking vs. friction loss for JPCP with different subgrade stiffness**

The terminal IRI graph shows that slabs with a joint spacing of 18' and 4000 subgrade resilient modulus performed better than pavements with stiffer bases except the section with 10" thickness. Both the 8,000 and 12,000 psi subgrades showed very similar performance with an 18' joint spacing. For pavements with a joint spacing of 12' and 15', increasing the resilient modulus to 12000 psi results in less terminal IRI compared to slabs with softer subgrades. For transverse cracking all the pavement sections showed similar trends in behavior. As the subgrade modulus was decreased then less cracking was observed compared to the other sections.

### **5.3 SUMMARY**

The documentation for Darwin ME states that the base parameters are not well understood and need to be better quantified. The sensitivity analysis performed clearly shows that in JCPC with higher joint spacing and in all CRCP pavements investigated that the base friction was an important parameter. Apparently there has been very few previous measurement of base friction made on concrete pavements. This would be a useful parameter to determine to help the state of Oklahoma adopt Darwin-ME and to help in improving the development of the software.

## CHAPTER 6 - A COMPARRISON BETWEEN FIELD INVESTIGATION AND PREDICTED PERFORMANCE FROM DARWIN-ME

In this chapter the research team compares the performance of a number of CRCP sites as well as the performance of several LTPP sites to the predicted performance in DARWIN-ME.

### **6.1 Investigation of Oklahoma CRCP**

Under a previous ODOT sponsored research project the OSU research team investigated a number of CRCP in the state of Oklahoma to investigate their performance and the correlation with y-cracking. This means that the research team already had a significant amount of field data about the performance of the CRCP. This meant that the team was able to focus on modeling the performance of the pavements in DARWIN-ME and then making a comparison. **Table 13** gives a summary of the sites investigated including the county, project number, highway, and project length.

**Table 13 - Summary of the CRCP pavements investigated.**

No.	County	Project No.	Route	Length (miles)
1	Logan	IR-35-4(115)147	35	10.56
2	Oklahoma	IR-35-3(073)123	35	1.74
3	Cleveland	IM-NHIY-35-2(221)(247)120	35	1.76
4	Cleveland	IM-NHIY-35-3(108)119	35	1.56
5	Carter	IMY-35-1(127)024	35	9.26
6	Okfuskee	IR-40-5(169)226	40	9.40
7	Atoka	F-299(99)	69	2.62
8	Atoka	F-299(45)	69	1.37
9	Atoka	F-299(35)	69	4.23
10	Pittsburg	MAF-186(183)	69	6.96
11	Pittsburg	MAF-186(185)	69	12.04
12	Pittsburg	DPIY-204(001)	69	7.28

A comparison between the results of the models and the measured performance is given in **Table 14**. With the exception of two projects there appears to be very good agreement with the predicted punchouts measured and the one predicted by Darwin-ME. One project where there was not good agreement was Okfuskee IR-40-5(169)226. This was an experimental pavement where in one direction there was no transverse steel used. This resulted in 58 punchouts/mile in the section with no transverse steel and only 7 punchouts/mile for the section with transverse steel. Darwin-ME was not able to predict the 58 punchouts because it was not possible to remove the transverse steel in the program. It is very interesting that Darwin-ME did predict 7.6 punchouts/mile. This closely matches the section where the transverse steel was used.

The other project where there was a difference observed was Atoka project F-299(35). Based on past conversation with ODOT officials it appears that this project had many challenges during the construction of this project. These challenges likely caused the high number of punchouts that were observed.

Despite these few differences, there seems to be overall agreement between the observed performance in the field and the performance predicted by Darwin-ME for CRCP with the default values in the program.

**Table 14 - The table shows a comparison to the punchouts measured and those predicted by Darwin-ME**

County	Date Opened	Thickness	Shoulder Type	Punchouts measured		MEPDG predictions
				AVG patch/mile		Punchouts/mile
				NB	SB	
Logan	1988	10	JPCP	0	5	2.81
Oklahoma	2001	10	CRCP	0	1	2.77
Cleveland 1	2002	10	CRCP	0	0	2.76
Cleveland 2	2005	10	CRCP	0	0	2.74
Carter	2007	12	JPCP	0	0	2.62
Okfuskee	1985	9	JPCP	7	58	7.65
Atoka 1	1989	10	JPCP	4	11	2.77
Atoka 2	1986	9	JPCP	3		2.67
Atoka 3	1986	9	JPCP	20	32	2.67
Pittsburg 1	1991	10	JPCP	1	0	2.81
Pittsburg 2	1989	10	JPCP	0	1	2.81
Pittsburg 3	1994	10	JPCP	1	1	2.81
Noble	1988	10	JPCP	5.1	3	2.84
Washita	1992	10	JPCP	6.4	3.6	2.75

## 6.2 Investigation of LTPP database sites

As part of this work the research team is also working on investigating concrete pavement sites that are also part of the LTPP database. There are five sites in Oklahoma. Three of them are CRCP and two are JCP. The team has gathered the information needed for the inputs into Darwin-ME. These are given in **Table 15**. In addition, the research team has visited a number of the sites to confirm the condition reported in the LTPP database. As can be seen from the database these pavement sections are performing quite well and do not show much damage. This was confirmed in the visual inspections of the highways. One item that still needs to be done is to investigate these sections in Darwin-ME and compare the predicted performance with the actual. This will be done before the final version of the document is submitted.

**Table 15 - Inputs for Darwin-ME for Oklahoma concrete LTPP sites.**

	Surface Type	CRCP Sections			JPCP sections	
	Section	40-4155	40-4158	40-5021	40-4157	40-4160
<b>Structure</b>	County	WASHINGTON	WASHINGTON	MAYES	MAYES	PONTOTOC
	Route/Direction	U. S.-75, North Bound	U. S.-75, South Bound	State-33, West Bound	U. S.-69, North Bound	State-3W, West Bound
	No. of Lanes	2	2	2	2	2
	Study	Unbonded PCC Overlay of PCC Pavement	Continuously Reinforced Concrete Pavement (CRCP)	Continuously Reinforced Concrete Pavement (CRCP)	Jointed Plain Concrete Pavement (JPCP)	Jointed Plain Concrete Pavement (JPCP)
	Age (years)	43	24	26	28	34
	Avg. Annual Daily Traffic (AADT)	3945	3945	5687	4736	1839
	Avg. Annual Daily Truck Traffic (AADTT)	387	723	651	1677	450
	Layer 1	Subgrade (untreated)	Subgrade (untreated)	Subgrade (untreated)	Subgrade (untreated)	Subgrade (untreated)
	Thickness, (in.)				42	
	Material Code Description	215-Coarse-Grained Soil: Silty Sand with Gravel	214-Coarse-Grained Soil: Silty Sand	265-Coarse-Grained Soil: Silty Gravel with Sand	214-Coarse-Grained Soil: Silty Sand	108-Fine-Grained Soils: Lean Clay with Sand
	Layer 2	Portland cement concrete layer	Bound (treated) base	Bound (treated) base	Bound (treated) base	Unbound (granular) subbase
	Thickness, (in.)	6.7	4.4	3.5	3.8	12
	Material Code Description	4-Portland Cement Concrete (JPCP)	319-HMAC	321-Asphalt Treated Mixture	319-HMAC	309-Fine-Grained Soils
	Layer 3	Asphalt concrete layer	Portland cement concrete layer	Portland cement concrete layer	Portland cement concrete layer	Bound (treated) base
	Thickness, (in.)	2.8	10.3	9.4	8.9	2.2
	Material Code Description	78-Dense Graded Asphalt Concrete Interlayer	6-Portland Cement Concrete (CRCP)	6-Portland Cement Concrete (CRCP)	4-Portland Cement Concrete (JPCP)	320-Sand Asphalt
	Layer 4	Asphalt concrete layer				Portland cement concrete layer
	Thickness, (in.)	0.9				9.2
	Material Code Description	78-Dense Graded Asphalt Concrete Interlayer				4-Portland Cement Concrete (JPCP)
	Layer 5	Portland cement concrete layer				
Thickness, (in.)	9.7					
Material Code Description	6-Portland Cement Concrete (CRCP)					
<b>Perf</b>	punchouts (count)	0	0	0		

Longitudinal Cracking (Length m)	0	0	0		
Transverse Cracking (count)	157	121	138	0	0
Spalling of long. Joints (length m)	0	0	0		
International Roughness Index (IRI) Section Average (m/km)	0.972	1.164	0.957	1.297	2.442
Faulting (mm)				0	4.6
Corner breaks (count)				0	0
Spalling of trans. Joints (length m)				1	2



# **CHAPTER 7 - A COMPARRISON BETWEEN FIELD INVESTIGATION AND PREDICTED PERFORMANCE FROM DARWIN-ME**

In this section work was done to investigate how the CTE and shrinkage of pavement mixtures change when different amounts of paste are used in the mixture. When optimized graded concrete is used then it allows one to reduce the paste or mortar content. The mixtures were prepared the same way described previously in the document with a dolomitic limestone and natural sand.

## **7.1 Coefficient of Thermal Expansion**

The results of the CTE versus the about of coarse aggregate content is shown in **Fig. 41**. The results show that as the coarse aggregate content is increased then the CTE of the concrete decreases. This suggests that optimized graded concrete with high coarse aggregate contents could be a beneficial tool to reduce the CTE of the concrete mixtures.

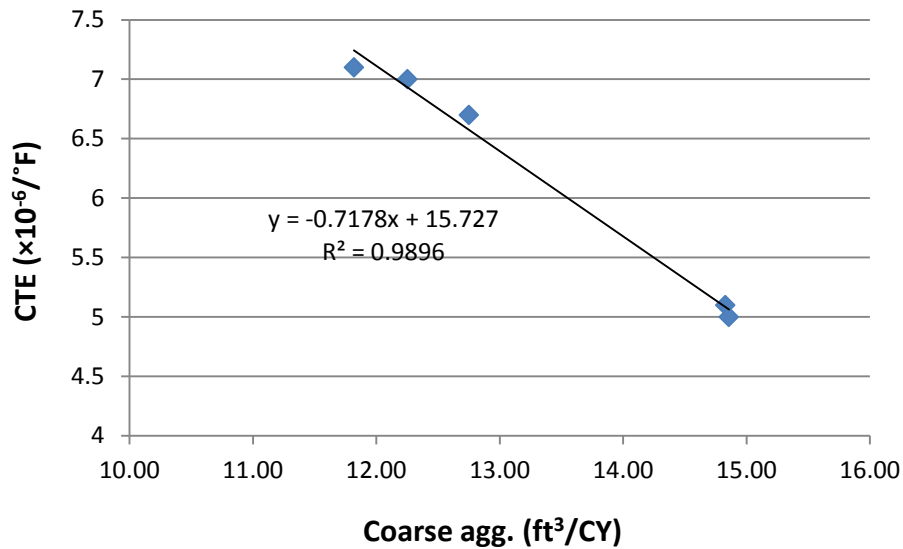


**Figure 41 - The CTE value for concrete mixtures with different amounts of coarse aggregate.**

## 7.2 Shrinkage

ASTM C157/C-04 was used as the procedure for testing the samples. After each mixture was tested for air content, three concrete prisms were made and placed in lime water for 28 days. Then each sample was measured using a comparator. Next the samples were placed in an environmental chamber at 74°F and 40% relative humidity. Length and weight change measurements were taken every month for 150 days. **Figures 42** and **43** compare the effects of shrinkage over time. **Figure 42** shows the expansion of the specimen over time, and **Fig. 43** shows the percentage of weight loss.

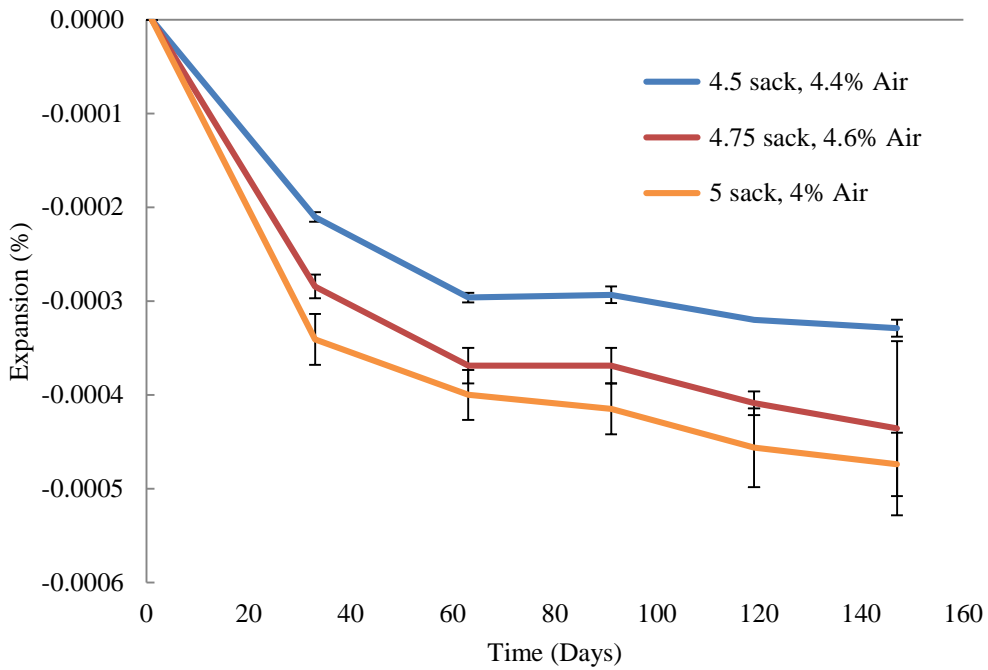


**Figure 42 - The expansion is shown over time for samples with different cement contents. A negative expansion means that the sample is shrinking.**

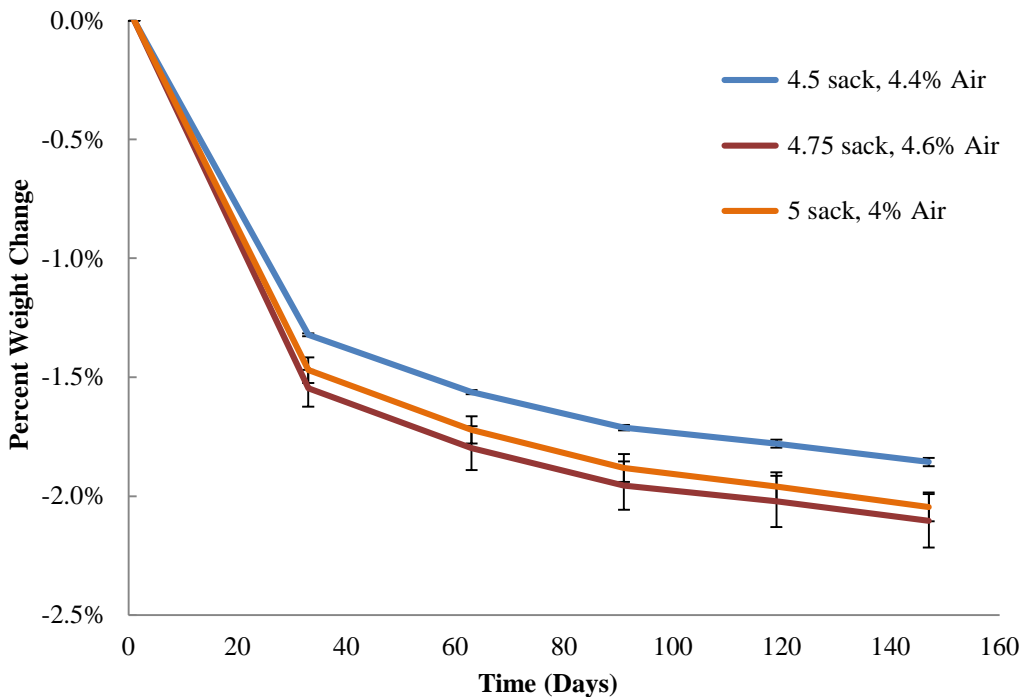


**Figure 43 - The weight loss of the samples over time when stored in a 40% relative humidity room.**

The shrinkage results clearly show that as the cement content is reduced in the mixture then the weight loss and overall shrinkage of the sample decreases. This

suggests that by using optimized graded concrete then the reduction in paste content should reduce the amount of shrinkage and the overall dimensional stability of the concrete. This in turn should reduce the amount of cracking in the member.

## CHAPTER 8 - CONCLUSIONS

A number of useful results have come from this research. They include:

- Increasing the wet curing length for concrete will increase the degree of saturation of fluid in the paste. This increased level of saturation will lead to increased strains on subsequent drying. Wet curing will also reduce mass transport. This will in turn lead to larger moisture gradients in the sample. All of this causes greater curling in wet cured paste and concrete samples. The models in Darwin-ME do not account for this and therefore need to be modified.
- If volume change is important for your concrete slab/pavement then it may be beneficial to limit the extent of wet curing. In a less severe environment, such as 70% RH, the same trends have been observed but the amount of predicted curling would not be significant. This means that if concrete is going to be used in dry conditions (~ 40% RH), then wet curing can lead to greater volume changes in the structure on drying. However, if the concrete is to be used in a moist environment, such as present in Oklahoma (~ 70% RH) then wet curing appears to have minimal impact on the volume change from drying. This means that wet curing shouldn't lead to increased volume change from drying and that it behaves similarly to no curing in laboratory curling experiments.
- The average RH in Oklahoma City is consistently 65% year round over the five year period investigated. This suggests that extreme drying environments are not likely applicable to concrete in this region. This means that the curling

of the concrete pavements is not sensitive to the curing method used in Oklahoma. This would not be the case in a climate with a lower average RH.

- The wet cured samples showed less mass change than the samples with curing compound and no curing.
- Surface of samples cured with PAMS based curing compound and resin based curing compound have not significantly changed after long term exposure, while surface of samples cured with water-wax based curing compound has been considerably eroded after five months of exposure.
- Different curing compounds perform very similarly in the above mentioned condition and strain changes are statistically similar, which were caused by continuous fluctuations in temperature and RH during the test.
- A pavement on I-44 in Tulsa was successfully instrumented. There does appear to be measurable curling occurring on the pavement. This curling seems to be likely caused by a significant moisture gradient that exists inside the pavement. The moisture gradient is likely caused by a high water table at the pavement.
- The sensitivity analysis performed with Darwin-ME on the impact of base friction on performance shows that in JCP with higher joint spacing and in all CRCP pavements investigated that the base friction was an important parameter.
- More work is needed to better understand useful assumptions for these parameters.

- Quantitative results have been provided on how the change in aggregate content of a mixture impacts the CTE and the ultimate shrinkage of concrete. Both of these indices show an improvement in performance as the paste concrete is reduced in the mixture.

In the next phase of the research the team will focus on bringing all of their findings together and to provide a final recommendation of how to implement Darwin-ME in Oklahoma.